


Hadronic structure on the light front. I. Instanton effects and quark-antiquark effective potentials

Edward Shuryak^{*} and Ismail Zahed[†]

Center for Nuclear Theory, Department of Physics and Astronomy,
Stony Brook University, Stony Brook, New York 11794–3800, USA

 (Received 15 August 2022; accepted 12 January 2023; published 24 February 2023)

This is the first of a sequence of papers that addresses the nonperturbative origin of the central and spin-dependent forces between quarks. Its main thrust is a focus on meson spectroscopy in the center-of-mass frame. We suggest a novel “dense instanton ensemble” model for the QCD vacuum, to explain the interquark forces in mesons, from quarkonia to heavy-light and light-light ones. The sequels will show how to export these interactions to the light front, and derive the corresponding Hamiltonians, mesonic, and baryonic light front wave functions. The ultimate aim of the series is to bridge the gap between hadronic spectroscopy and partonic observables.

DOI: [10.1103/PhysRevD.107.034023](https://doi.org/10.1103/PhysRevD.107.034023)

I. INTRODUCTION

The physics of hadrons is firmly based in quantum chromodynamics, a theory over half a century old. One might think that by now this subject has reached a solid degree of maturity with most issues settled. Unfortunately this is not yet the case. The field of nonperturbative QCD consists of several subfields, which can be defined as follows:

- (1) hadronic spectroscopy (masses and wave functions of mesons, baryons, pentaquarks, etc.);
- (2) QCD vacuum structure (vacuum condensates, Euclidean correlation functions, etc.); and
- (3) light-front observables (distribution amplitudes, parton distribution functions or PDFs, etc.).

They are relatively weakly connected, although in the past decade considerable efforts to bridge them has taken place.

Our current set of papers, in addition to this one [1–4], represent efforts in this direction. In this introductory section we will give a brief description of the first two aforementioned subfields. The third one will be discussed in the papers to follow, starting from [1].

A. Hadronic structure

This field originated in the early 1960s, and experienced a rapid expansion in the last decade, due to the discoveries

of multi-quark hadrons in the heavy-light sector. We will not discuss these “exotic hadrons” in this work but focus on the underlying physics at the origin of the interquark forces. Parametrizing and understanding them is a needed step, setting the stage for derivation of the effective Hamiltonians on the light front.

Early nonrelativistic quark models achieved resounding success, in part through simple formulas for the masses and magnetic moments of baryons made of light quarks. The revolutionary discoveries in the 1970s of “quarkonia,” the bound states made of heavy c , b quarks, revealed families of narrow bound states well described by the celebrated Cornell potential

$$V_{\text{Cornell}}(r) = -\frac{4\alpha_s}{3} \frac{1}{r} + \sigma_T r. \quad (1)$$

Further theory effort developed effective nonrelativistic theories, such as nonrelativistic QCD (NRQCD) and perturbative nonrelativistic QCD (pNRQCD). They put spectroscopy of quarkonia close to that of atoms and nuclei in accuracy. A number of universal (flavor independent) central and spin-dependent potentials were defined, expressed via certain nonlocal correlators of vacuum gauge fields. For a short but concise summary see e.g. [5].

The Cornell potential attributes the short-distance potential to perturbative one-gluon exchange, and its large distance $\mathcal{O}(r)$ contribution to the tension of the confining flux tube (QCD string). The issues to be discussed in this paper are the nonperturbative origins of the interquark interaction at *intermediate* distances $r \sim 0.2\text{--}0.5$ fm. Those are especially important for small size hadrons, such as bottomonia or pions (see below).

^{*}edward.shuryak@stonybrook.edu

[†]ismail.zahed@stonybrook.edu

Published by the American Physical Society under the terms of the [Creative Commons Attribution 4.0 International license](https://creativecommons.org/licenses/by/4.0/). Further distribution of this work must maintain attribution to the author(s) and the published article's title, journal citation, and DOI. Funded by SCOAP³.

A static quark potential $V_C(r)$ is defined through a vacuum average of a pair of parallel Wilson lines,

$$e^{-V_C(r)T} = \langle W(\vec{x}_1)W^\dagger(\vec{x}_2) \rangle \quad (2)$$

defined by

$$W(\vec{x}) = \text{Pexp} \left(ig \int_W dx_4 A_\mu^a(x_4, \vec{x}) \hat{T}^a \right) \quad (3)$$

where color generator $\hat{T}^a = t^a/2$, with t^a Gell-Mann matrices. Pexp is a path-ordered matrix product. The parallel lines are running in the Euclidean time direction, separated by the spatial distance $r = |\vec{x}_1 - \vec{x}_2|$. The lines are connected at times $\pm T/2$, but eventually the limit of large time $T \rightarrow \infty$ is assumed; making connectors unimportant. Historically, the derivation of this potential has been at the forefront of lattice studies of the QCD vacuum. In a way, it is similar in spirit to the Born-Oppenheimer approximation in molecular physics, where the probe quarks backreaction is ignored. For recent developments and references, we refer to the work by Brambilla *et al.* [6].

Traditionally, the central potential was used as linear $V_C(r) = \sigma_T r$ with σ_T being the tension of the confining flux tube (known also as the QCD string). So, one might think the issue of the central potential is very simple. Unfortunately, it is far from being so, and there are several impediments for usage of the flux tubes.

The first is that the simple linear term is expected to be correct at large distances only, while at smaller r there are other nonperturbative effects as well. The simplest corrections are due to quantum vibrations of the flux tube. The first of them is the famous ‘‘Lusher term,’’ attractive $\sim 1/r$. If the string is described by a Nambu-Goto geometrical action, these vibrations are summed up in the so-called Arvis form [7]

$$E(r) = \sigma_T r \sqrt{1 - \frac{\pi}{6} \frac{1}{\sigma_T r^2}}. \quad (4)$$

This expression predicts that potential vanishes at $r \approx 1/3$ fm. Furthermore, the QCD string may have a much more complicated action, so the Arvis potential cannot be really trusted when the corrections are large. Yet the two first expansion terms are universal, see more in [8]. Lattice studies of these corrections (e.g. [9]) in the setting with two static charges, or a flux tube wrapped around the lattice, do confirm these two terms.

An important issue to be discussed is the derivation of the relativistic corrections $\sim (v/c)^2 \sim (\Lambda_{\text{QCD}}/m_Q)^2$ where m_Q is a heavy quark mass and Λ_{QCD} stands for a ‘‘QCD scale.’’ Such perturbative terms are well known in atomic and nuclear physics, and changing from one-photon to one-gluon exchange is simple. So it is clear how spin-spin,

spin-orbit, and tensor force V_{SS}, V_{SL}, V_T arise from perturbative contributions, being all just certain derivatives of the Coulomb potential.

The question is what are the nonperturbative contributions to these potentials. Those can be related to Wilson lines decorated by two extra field strengths [10,11]. Schematically, they have the form

$$\langle W G_{\mu\nu}(x) W W^\dagger G_{\mu\nu}(y) W^\dagger \rangle.$$

More details of the invariant spin potentials are given in Appendix B.

In a nonrelativistic setting, spin-dependent forces originate from quark (gluo-)magnetic moments interacting with vacuum fluctuations of (mostly) *gluo-magnetic* fields. Unfortunately, the QCD flux tubes carry *electric* flux: models of their structure and lattice studies specify mostly distribution of the gluo-electric fields in them, not the gluo-magnetic ones needed for the spin forces. So, one has to think about other origins of those in the vacuum.

In principle, the pertinent correlation functions can be calculated on the lattice, so one might think that all spin-dependent forces are by now well documented and their origins explained. Unfortunately, this is not the case as quantitative lattice studies have only started recently. Below we will investigate to what extent such correlators, evaluated using certain models of vacuum fields, can reproduce the observed spin-dependent potentials. We will find that in heavy quarkonia instanton-induced forces can provide contributions to perturbative ones, leading together to a good description of splittings for a number of the low-lying states.

However, for spin splittings in light quark states these forces coming from Wilson lines are not sufficient. The resolution comes from additional terms in the quark propagator, related to their disappearance/creation in/from the Dirac sea. In Euclidean space-time a semiclassical description of gauge field vacuum is technically described by parts of the propagators built out of fermionic zero modes. In other words, these spin forces are induced by a ‘t Hooft effective Lagrangian for light quarks.

In Fig. 1 we show schematically how these vertices contribute to the pion and rho meson correlation functions. The instanton-induced four-quark effective interaction, derived by ‘t Hooft using the fermionic zero modes, has the chiral-flavor structure $(\bar{u}_R u_L)(\bar{d}_R d_L)$. For the anti-instantons, the left and right spinor components are interchanged. The upper illustration in Fig. 1 shows that for the π^+ propagation, the alternating ‘t Hooft instanton and anti-instanton vertices can be directly iterated, in the mean-field approximation. In the π^0 channel, the ‘t Hooft vertex acts in the annihilation channels

$$\bar{u}_R u_L \rightarrow \bar{d}_R d_L \rightarrow \bar{u}_R u_L \dots$$

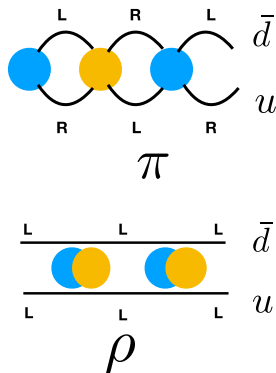


FIG. 1. Schematic representation of the role of instanton-induced 't Hooft Lagrangian in the structure of the pion (top) and rho meson (bottom). In the latter case effective four-fermion operator corresponds to combined instanton and anti-instanton vertices.

These processes make the pion massless, and the η , δ heavy, owing to the attraction and repulsion of the 't Hooft vertices in these channels; see [12].

The lower illustration in Fig. 1 shows how the 't Hooft vertices contribute to the ρ^+ vector/axial (correlation functions). The vector currents have the same chirality for the quark-antiquark pair, while the instanton zero modes generate quark-antiquark vertices of opposite chirality. Therefore one has to go to the next order in the instanton density, with effective interactions that are second order in the 't Hooft Lagrangian. More specifically, by nesting these vertices and contracting inside the loop the right u_R and \bar{u}_R , as well as the right d_R with \bar{d}_R , we have

$$(\bar{u}_R u_L)(\bar{d}_R d_L) \times (\bar{u}_L u_R)(\bar{d}_L d_R) \rightarrow (\bar{u}_L u_L)(\bar{d}_L d_L)$$

with the left chirality left uncontracted. The resulting operator is chirality preserving (conserved axial charge), since an instanton-anti-instanton pair as per the illustration has zero topological charge. We will return to the light vector ρ mesons in Sec. IV E. The analytic form of the effective second-order four-fermion operator will be given in (87).

B. QCD vacuum and instanton liquid model

Nonperturbative physics of strong interactions started before the development of QCD in the 1970s. Nambu and Jona-Lasinio (NJL) [13], inspired by BCS theory of superconductivity, have qualitatively explained that strong enough attraction of quarks can break $SU(N_f)_A$ chiral symmetry spontaneously and, among many other effects, create near-massless pions. Chiral effective Lagrangians and related theory have lead to one important input, a nonzero quark condensate $\langle \bar{q}q \rangle \neq 0$.

The discussion of the QCD vacuum structure started with the QCD sum rules [14], where the short-distance

description of Euclidean point-to-point correlation functions via the operator product expansion (OPE) was related to their long-distance description in terms of the lightest hadrons. The (Euclidean) correlators of QCD operators were calculated in terms of the leading vacuum condensates, $\langle G^2 \rangle$, $\langle \bar{q}q \rangle$, etc. Yet it was soon realized that the strongest nonperturbative effects (in the scalar and pseudoscalar channels) are *not* described by the “mean field” OPE predictions [15].

Extensive studies of point-to-point (Euclidean) correlation functions in multiple mesonic channels, based on phenomenology [16], have indeed found striking differences between correlators of operators with different quantum numbers. While for vector currents ($\bar{q}\gamma_\mu q$) made of *light* quarks $q = u, d, s$ only small deviations from free quark propagation is observed; correlators of the scalar and pseudoscalar operators ($\gamma_\mu \rightarrow 1, \gamma_5$) show strong splittings from them at surprisingly small distances. As shown in detail in [16], these splittings found their explanation in terms of topological fluctuations of gluonic fields, described semiclassically by instantons [17].

The semiclassical model of the QCD vacuum structure based on instantons [18] is known as the instanton liquid model (ILM). It introduced an important scale parameter of the nonperturbative vacuum—the typical instanton size

$$\rho \sim \frac{1}{3} \text{ fm.} \quad (5)$$

Because it is rather small compared to the size of most hadrons (except for the lowest Υ 's and the pion, see below), where possible we will use a *quasilocal* approximation in which it is going to zero.

In the ILM the vacuum fields are very inhomogeneous: blobs of strong gauge fields (at the instanton centers) surrounded by “empty” space-time, free from nonperturbative fields. Since the mid-1990s such field distributions were obtained from lattice configurations by means of various “cooling” methods. A picture is better than many words, so we reproduce in Fig. 2 one visualization of the topological charge distribution from [19–21] which reveals a number of instantons and anti-instantons.

Note that the topological clusters are also threaded by a thin center vortices or Z_3 -fluxed strings, which span worldsheet surfaces in four dimensions. While the center vortices are important for enforcing confinement at long distances, Fig. 2 shows that they are on average decoupled from the inhomogeneous and strong topological fields. Moreover, their field strength in the vicinity of these topological fields is about $\sigma_T \bar{\rho} \approx 0.3 \text{ GeV}$, which is weaker than the typical chromoelectric or chromomagnetic field in the instanton center $\sqrt{E} = \sqrt{B} \approx 2.5/\bar{\rho} \approx 1.5 \text{ GeV}$, but crucial for long-distance color correlations.

Instantons are not just semiclassical solitons made of glue. As discovered by 't Hooft [23], they generate four-dimensional fermionic zero modes which lead to a

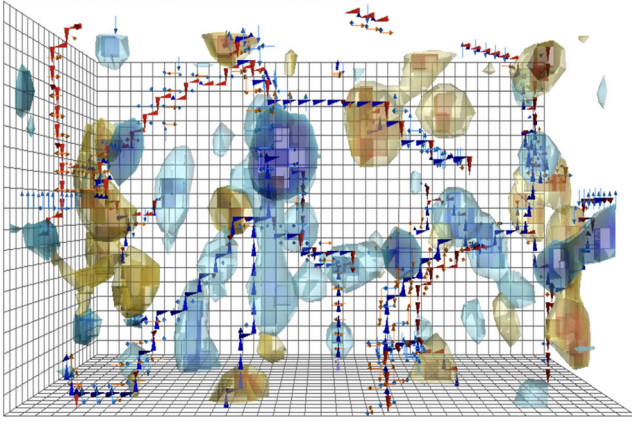


FIG. 2. Instantons (yellow) and anti-instantons (blue) configurations in the “deep-cooled” Yang-Mills vacuum. After center projection, they are threaded by center P-vortices [20,21]. They constitute the primordial gluon epoxy (hard glue) at the origin of the light hadron masses [22]. The center P-vortices are responsible for confinement. See text.

multifermion effective Lagrangian. The instanton-induced four-quark not only solves the famous “ $U_A(1)$ problem”—by making the η' non-Goldstone and heavy—but it also produces a strong attraction in the σ and π channels. Including those in the framework of the ILM [24] one gets a microscopic understanding of chiral symmetry breaking, chiral perturbation theory, the pion properties etc. The 't Hooft instanton-induced effective Lagrangian is a QCD substitute to the hypothetical Nambu-Jona-Lasinio [13] four-quark interaction.

Another version of this theory look at quarks “hopping” from one instanton to another. The resulting loops in the quark determinant can be either short or long (infinite in thermodynamic limit $V_4 \rightarrow \infty$). The latter component is responsible for the localization of the Dirac eigenvalues close to zero $\lambda \sim 1/V_4$.

Two parameters of the original ILM are the size and the density of instantons

$$\rho = \frac{1}{3} \text{ fm}, \quad n_{I+\bar{I}} = \frac{1}{R^4} = 1 \text{ fm}^{-4} \quad (6)$$

which in turn defines the so-called diluteness parameter

$$\kappa \equiv \pi^2 \rho^4 n_{I+\bar{I}}. \quad (7)$$

So, the ILM predicts it to be small $\kappa_{\text{ILM}} \sim \mathcal{O}(1/10) \ll 1$. These parameters have withstood the scrutiny of time, and describe rather well the chiral dynamics related to pions, the Euclidean correlation functions in the few femtometers range, and much more; see [12] for a review.

Another formulation of chiral symmetry breaking relates it to the *collectivization* of the instanton zero modes, into the so-called zero mode zone (ZMZ). Due to nonzero

matrix elements of the Dirac operator, near-zero Dirac eigenvalues are residing within a strip of small width

$$|\lambda| \sim \text{width (ZMZ)} \sim \frac{\rho^2}{R^3} \sim 20 \text{ MeV} \quad (8)$$

as predicted by the original ILM with the parameters given above (6). In [25] the meson and baryon spectroscopy was studied, with all Dirac states inside a certain strip of eigenvalues $|\lambda| < \Delta$ eliminated. A strong restructuring of the light hadronic spectra was indeed observed if $\Delta > \text{width (ZMZ)}$. In particular, the Nambu-Goldstone modes (pions) totally disappear from the spectra, as expected. It would be interesting to extend the same analysis to the heavy-light sectors, and to address more generally what happens with all forms of spin-dependent forces.

Further statistical description of interacting instanton ensembles was developed by mean field methods and statistical simulations; for review see [12]. Some related lattice studies are [26,27].

C. Topological landscape and $I\bar{I}$ molecules

The “landscape” refers to the minimal energy gauge field configurations, as a function of two main variables. The first is the topological Chern-Simons number

$$N_{\text{CS}} \equiv \frac{e^{a\beta\gamma}}{16\pi^2} \int d^3x \left(A_\alpha^a \partial_\beta A_\gamma^a + \frac{1}{3} \epsilon^{abc} A_\alpha^a A_\beta^b A_\gamma^c \right). \quad (9)$$

For the second we will use the rms size of the configuration, related to the field strength

$$\rho_{\text{rms}} = \frac{\int r^2 G^2 d^3r}{\int G^2 d^3r}. \quad (10)$$

For fixed ρ , the landscape is shown in Fig. 3. It has been defined in Ref. [28] and is given in a parametric form,

$$U_{\text{min}}(\kappa, \rho) = (1 - \kappa^2)^2 \frac{3\pi^2}{g^2 \rho},$$

$$N_{\text{CS}}(\kappa) = \frac{1}{4} \text{sign}(\kappa) (1 - |\kappa|)^2 (2 + |\kappa|) \quad (11)$$

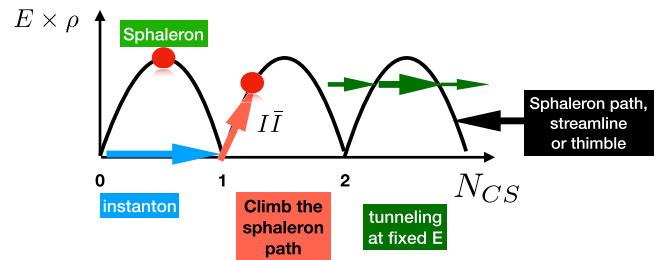


FIG. 3. The topological landscape: minimal energy (times rms size) versus Chern-Simons number N_{CS} (left); thimble path (center); tunneling at nonzero energy (right).

with parameter κ . At $\kappa = \pm 1$ the minimal energy is zero, while $\kappa = 0$ corresponds to a maximum of the energy. This point was called “the sphaleron” in electroweak theory [29]. The set of configurations at arbitrary κ is called the sphaleron path. Those consist of static 3d magnetic field configurations, known also as the turning points (by analogy to points in quantum mechanics where the semiclassical momentum vanishes).

The (anti-)instanton is a tunneling path connecting the *bottoms* of two subsequent valleys, at energy zero. Since they have topological charge $Q = \pm 1$, they result in change of Chern-Simons number $\Delta N_{CS} = \pm 1$.

However instanton paths are not the only form of topological fluctuations which may occur in this landscape. Indeed, we will discuss *two* additional sets of paths: (i) those that travel the landscape along the sphaleron path (or “streamline”); and (ii) those that travel the landscape at fixed energy, including the tunneling, all of which are illustrated in Fig. 3.

The first set is described by a constrained Yang-Mills equation with a nonzero right hand side, or external current, which drags them up (or down) the potential along the gradient. In the mathematical literature this construction is known as “Lefschetz thimbles,” a special path connecting two extrema of a function following its gradient. In QCD-related literature they are known as “streamline” configurations described by overlapping instanton–anti-instanton pairs or molecules.

The second set is described by a Yang-Mills equation with a *zero* right hand side, and thus is occurring at fixed energy. The path’s history passes the turning points *twice*, with Euclidean time solution in between them, known as tunneling at nonzero energy. In general, those should be complemented by Minkowskian time solutions, before and after turning points. The technical name for those is “zigzag path” indicating a turn from real to imaginary time and then back to real.

Both sets of solutions, with proper references, are detailed in the appendices. What we would like to emphasize here the fact that they describe gauge field fluctuations *different from* well-separated instantons. They are neither self-dual nor possess (near) zero Dirac eigenvalues—and therefore they do not contribute to chiral symmetry breaking and were not included in the original ILM. And still, they do describe certain fluctuations of vacuum gauge fields, and therefore can contribute to certain observables, especially the Wilson lines. Therefore, we will investigate their contributions to central and spin-dependent forces between quarks. The inclusion of molecules or zigzag paths is the novel element of the novel vacuum model we develop here.

Close instanton–anti-instanton pairs are of course known, and in particular they were observed on the lattice. They are however not seen in Fig. 2 obtained by so-called “deep cooling” of configurations, during which close instanton–anti-instanton pairs are already annihilated. The application of the “molecular component” of the vacuum was made

previously in connection to phase transitions in hot/dense matter. Indeed (if quark masses are neglected), this component is the only one which survives at temperatures $T > T_c$, where chiral symmetry is restored. Accounting for “atomic” and “molecular” components together started with [30]. The molecular component was also shown to be important at high baryonic densities, where it contributes to quark pairing and color superconductivity [31]. More recently, we have explored it in the context through nonperturbative contributions to the mesonic form factors [32] and matching kernels [33].

The theory of sphaleron processes (sketched in the middle of Fig. 3) is related to the issue of $I\bar{I}$ interaction. Numerical calculation of the “streamline” along the action gradient was first done for quantum-mechanical instantons in [34], for gauge theory the streamline equation was derived in [35], solved approximately by [36], and numerically by [37]. The surprising finding of the latter paper was that “Yung ansatz” was rather accurate not only at large distances $R \gg \rho$ between instanton and anti-instanton, where it was derived, but in fact for any distance till zero. Note that the last two papers used conformal inversion at the center of the instanton, making I and \bar{I} co-central.

Consider I and \bar{I} of the same size ρ and same color orientation, with 4-distance between their centers R serving as the parameter of the set, with $x_{1\mu} = (0, 0, 0, R/2)$, $x_{2\mu} = (0, 0, 0, -R/2)$. In the mathematical literature such a set is known as *Lefschetz thimble*; it connects one extremum at large R , the independent I and \bar{I} , with another, the zero field at $R = 0$. Note that at the locations $y_4 < 0$ the gauge fields are approximately anti-self-dual $\vec{E} \approx -\vec{B}$, and at $y_4 > 0$ they are approximately self-dual $\vec{E} \approx \vec{B}$. At $y_4 = 0$ the electric field vanishes. As shown in [28], these 3d magnetic objects obtained using Yung ansatz are very close to the sphaleron path configurations obtained by constrained energy minimization.

The instanton–anti-instanton streamline therefore provides a semiclassical description of the sphaleron production. In the context of electroweak theory it was first used in [38,39] three decades ago. Recent interest in the production of QCD sphalerons at the LHC and RHIC is discussed in our recent paper [40].

Let us now move to lattice observables, to which the molecular component of the instanton ensemble contributes, the simplest of which is the so-called gluon condensate $\langle G_{\mu\nu}^2 \rangle$ introduced in the context of the QCD sum rules framework [14]. The accuracy of this number was later questioned and it was revised to a larger value. Further discrepancies were shown in lattice studies, that were attempting to extract local (or nonlocal) observables with powers of the gauge field strength $G_{\mu\nu}$.

Nowadays, when “cooling” by the gradient flow method can be consistently related to the renormalization group flow [41], one can put the appropriate scale dependence of the molecular component on a firm basis. Skipping several

decades, let us take as an example the recent work [42] which studies the 3- and 4-point gluon field correlators and relates their evolution to topology during cooling. Their original motivation was to extract the gluon coupling $\alpha_s(k)$, so the observable was chosen to be the ratio of the 3-point to 2-point Green's function leading to effective coupling

$$\alpha_{\text{MOM}}(k) = \frac{k^6 \langle G^{(3)}(k^2) \rangle^2}{4\pi \langle G^{(2)}(k^2) \rangle^3}. \quad (12)$$

In the “uncooled” quantum vacuum (with gluons) the effective coupling starts running downward at large $k > 1$ GeV, as expected by asymptotic freedom. However at low $k \rightarrow 0$, one finds another persisting positive power of k , with a slope that matches exactly the one following from an instanton ensemble [43]

$$\alpha_{\text{MOM}}(k) \rightarrow \frac{k^4}{18\pi n_{I+\bar{I}}}. \quad (13)$$

Furthermore, it was observed that with increasing cooling time τ , the same power spreads to higher momenta, $k > 1$ GeV. It was observed that cooling eliminates not only perturbative gluons, but close instanton–anti-instanton pairs as well.

The dependence of the mean instanton sizes and density as a function of the (gradient flow) cooling time is shown in Fig. 2, from [42]. Their main conclusion is that the size and density of instantons in the vacuum, extrapolated to zero cooling time ($\tau \rightarrow 0$)—are approximately

$$\rho \rightarrow \frac{1}{3} \text{ fm}, \quad n \rightarrow 10 \text{ fm}^{-4}. \quad (14)$$

Therefore one can see that total instanton density is significantly larger than known before from deep cooling (large τ) of $1/\text{fm}^4$, as in the original ILM. In fact, the density may even be larger than that, because the definition of instantons used in this paper exclude pairs (molecules) which are too close. We will use these numbers, as indicative, for our dense instanton liquid model below.

D. Content of this paper

In Sec. II we will argue that the *upper* limit on the total instanton density can be deduced from known magnitude of the central potentials, e.g. from quarkonium spectroscopy.

The main purpose of the present paper is to quantify nonperturbative spin-dependent forces. We begin by reviewing their phenomenology in Sec. III A and then the theory in Sec. III D which is based on the standard “Wilson lines plus two field strengths” correlators. The contribution of an instanton to a pair of Wilson lines can be readily calculated analytically. This approach has been first used to calculate the static $\bar{Q}Q$ potential by the original Princeton group [10]. Two decades later we generalized it to high energy $\bar{Q}Q$ and dipole-dipole scatterings [44]. In

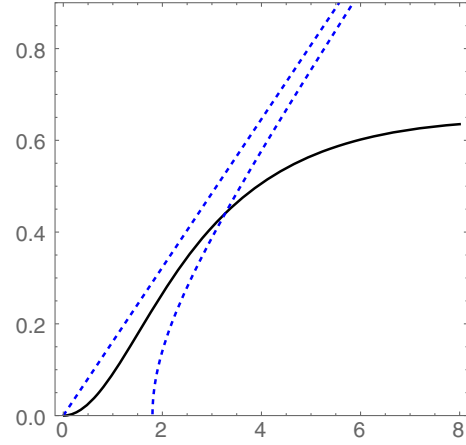


FIG. 4. Comparison of the central potentials $V_C(r)$ versus the interquark distance r in GeV^{-1} (so $1 \text{ fm} \approx 5 \text{ GeV}^{-1}$ on this plot). The solid line is the one derived from the “dense” instanton ensemble. The potential produced by the confining flux tube is illustrated by two blue dashed lines; the upper linear line is the classical string, and the lower is the Arvis potential (4) accounting for quantum string vibrations [7].

the scattering approach, the Wilson lines are first assumed to cross at an angle θ_{12} in Euclidean geometry. The final result is analytically transformed to a scattering amplitude (near) the light front by the substitution of the angle θ_{12} between two Wilson lines, to the hyperbolic angle $i\eta$ with relative rapidity y between two colliding particles in the ultrarelativistic limit. Unfortunately, neither of these works were widely noticed or actually used by phenomenologists (except for [45,46]).

An extensive study of the instanton-induced effects on heavy quarkonia has been revived recently by Musakhanov *et al.* (see e.g. [47]), who calculated the magnitude of the effect for the central as well as the spin-spin, spin-orbit, and tensor forces. Using the original ILM parameters of [48], it was found that the central potential is of magnitude ~ 150 MeV at large r , a relatively small correction to the phenomenological potential. The spin-spin potential was also calculated, and was found to be short ranged and of order of about 30 MeV, also a small correction. The spin-orbit and tensor forces are even smaller.

We will modify these results by using our new model for the instanton ensemble, and compare the results to the lattice results for spin-spin forces in Sec. III C, and to the phenomenological vector-pseudoscalar mass splittings in Sec. III D. We will see that in this setting the splittings in heavy-heavy quarkonia are reproduced.

The next challenge using the novel model is to extend the same analysis to heavy-light mesons such as B, D, \dots , and eventually light-light mesons. The goal is to find out whether these lighter systems can also be described analogously using variants of the “constituent quark” models.

Not all instanton-induced effects are included using temporal Wilson loops with straight fermion lines. The

part of the quark propagation, related to the chiral anomaly, instanton zero modes, and the 't Hooft Lagrangian has to be treated separately as we detail in Sec. IV. Only the inclusion of this effective interaction can describe pions.

Yet to get the correct mass and wave function of the vector (ρ) mesons, we also need the effective forces originating from $I\bar{I}$ molecules; see Sec. IV E. The discussion of the heavy-light systems is in Sec. IV F. The conclusions reached in this study are summarized in Sec. V.

II. CENTRAL POTENTIALS

A. Flux tubes versus the instantons

The static quark potential $V_C(r)$ is defined via the vacuum average of the Wilson line

$$W = P \exp \left[ig \int dx^\mu A_\mu^a \hat{T}^a \right] \quad (15)$$

over a closed rectangle $r \times T$. In the limit when the time extent is much larger than the spacial extent $T \gg r$, one can ignore the small integrals over the spatial direction $r = |\vec{x}_1 - \vec{x}_2|$, and keep only two over the Euclidean time direction, defining the potential by

$$e^{-V_C(r)T} = \langle W(\vec{x}_1)W^+(\vec{x}_2) \rangle. \quad (16)$$

For decades this Wilson's definition has been used in lattice studies.

We already noted that due to quantum vibrations of the QCD string, the flux tube contribution to $V_C(r)$ is in fact

$$I(x) = \int_0^\infty dy y^2 \int_{-1}^1 dc \left[1 - \cos(\alpha_1) \cos(\alpha_2) - \frac{y + xc}{\sqrt{y^2 + x^2 + 2xyc}} \sin(\alpha_1) \sin(\alpha_2) \right] \quad (18)$$

in which c is the cosine of the angle between \vec{r} and \vec{y} , going through the instanton center. The two color rotation angles are

$$\alpha_1 = \pi \frac{y}{\sqrt{y^2 + \rho^2}}, \quad \alpha_2 = \pi \sqrt{\frac{y^2 + x^2 + 2xyc}{y^2 + x^2 + 2xyc + \rho^2}}. \quad (19)$$

Note that they vanish for zero impact parameter of the line $y = 0$ and become π if their impact parameter gets large. In the former case the integrand above vanishes as $\cos(\alpha) = 1$, in the latter $\cos(\alpha) = -1$ and the integrand is maximal.

Using the instanton parameters of the ILM (6) one finds the large distance value of about 150 MeV [47]. We however extend the original ILM including also a molecular $I\bar{I}$ component. As a first approximation (to be improved later) we will do so by just enhancing the density, keeping the

rather uncertain at the distance scale $\sim 1/3$ fm. Yet precisely this distance range happens to be the most important one for spin-dependent forces.

Another important point is that the quark spins, due to the magnetic moments, interact with *magnetic* fields. The spin-dependent potentials can be defined via the average of two Wilson lines to which either two magnetic field strengths or product of electric and magnetic fields are added. The QCD flux tubes description, however, provides a description of the *electric* fields only. Therefore, one might think that they cannot contribute significantly to the spin forces.

The instantons (anti-instantons) are self-dual (anti-self-dual) vacuum fluctuations, in which the modulus of the magnetic and electric fields are equal. Furthermore, the Belavin-Polyakov-Schwartz-Tyupkin (BPST) instanton fields have "hedgehog" structure $A_\mu^a \sim \eta_{\mu\nu}^a x^\nu$, and since along the straight line dx^μ is the same vector, the colors are rotated around the same direction. Therefore, the accumulated rotation angle is given by an integral along the line [10,11]. The instanton-induced central potential has the form

$$V_{\text{instanton}}(r) = \frac{4\pi n_{I+I} \rho^3}{N_c \rho} I\left(\frac{r}{\rho}\right). \quad (17)$$

Here n_{I+I} is the instanton plus anti-instanton four-dimensional density, ρ is the typical instanton size, and the function $I(x)$ is defined by an integral over the location of the instanton center y_μ ,

function with the same instanton size $\rho = 1/3$ fm [as justified by lattice data of Fig. 2(a) of [42]].

The molecular density n_{mol} should be limited from above by the phenomenological value of the central potential. The instanton contribution to $V_C(r)$ is shown in Fig. 4 (solid line) for

$$n \equiv n_{\text{mol}} + n_{\text{ILM}} = 7. \text{ fm}^{-4}. \quad (20)$$

Note that this density is about twice lower than indicated by a triangle and extrapolation lines in Fig. 2(b) of [42]. The instanton-induced central potential, shown in Fig. 4 by the black solid curve will play a central role for the determination of the spin-dependent potentials as well. For future reference, record the corresponding numerical values below, with the entries ($r(\text{GeV}^{-1})$, $V_{\text{inst}}(\text{GeV})$),

$$\begin{aligned}
&(0, 0), (.333, 0.0114), (0.666, 0.043), (1., 0.0912), (1.33, 0.147), (1.66, 0.207), (2., 0.265), (2.33, 0.31), (2.666, 0.368), \\
&(3., 0.410), (3.33, 0.447), (3.66, 0.479), (4., 0.506), (4.33, 0.529), (4.66, 0.548), (5., 0.565), (5.33, 0.579), (5.66, 0.591), \\
&(6., 0.601), (6.33, 0.610), (6.66, 0.617), (7., 0.623), (7.33, 0.628), (7.66, 0.632), (8., 0.635), (8.33, 0.637), (8.66, 0.639), \\
&(9., 0.641), (9.33, 0.642), (9.66, 0.642), (10., 0.642).
\end{aligned} \tag{21}$$

The instanton-induced central potential is quite close to the phenomenological linear potential, for not-too-large distances $r < 3 \text{ GeV}^{-1}$. Assuming it is indeed the case, we proceed to calculate the spin-dependent effects below, and will show that the results are quite reasonable.

Note further that, with this choice, the diluteness parameter $\kappa \approx 1$. In other words, the ensemble is very dense, with the mean interparticle distance as low as

$$R_{\text{dense}} \equiv n^{-1/4} = 0.61 \text{ fm} \approx 2\rho.$$

(It may appear too dense; but remember that the $I\bar{I}$ molecules are not in fact two independent instantons, and their fields and action are partially cancelling each other.)

But before we do so, let us take a well-studied example—the bottomonium states—and check to what extent the difference between the linear and instanton-induced potential at $r > 1 \text{ fm}$ is reflected in the mass spectra. We have

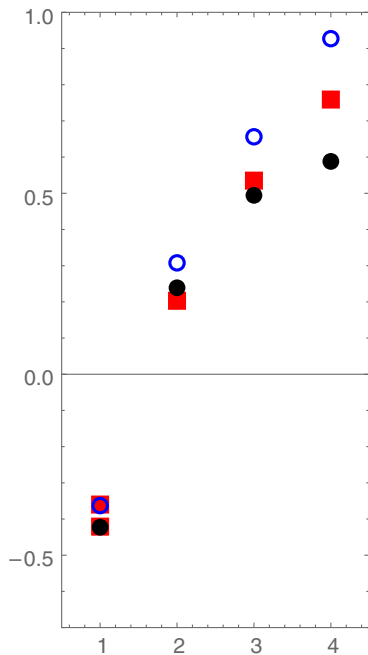


FIG. 5. Nonrelativistic energies $M_i - 2M_b$ for spin averaged $\bar{b}b$ states as a function of the principal quantum number n . Five red squares show the experimentally determined masses of $\Upsilon[1S]$, $\eta_b[1S]$, $\Upsilon[2S]$, $\Upsilon[3S]$, $\Upsilon[4S]$, the blue circles correspond to the standard Cornell potential, while the black closed circles are based on the instanton-induced potential shown in Fig. 4.

calculated the levels of bottomonium $\bar{b}b$ states using both potentials. In Fig. 5 we show their nonrelativistic energies for four radial excitations, with S -shell, orbital momentum $L = 0$. (The spin-dependent forces were not included—we return to those in the next subsections—therefore the calculation corresponds to the spin averaged combination, of $J = 1$ Upsilon and $J = 0$ η_b states.) The difference between these two potentials at large distances $r > 5 \text{ GeV}^{-1} \approx 1 \text{ fm}$ does indeed translate into different predictions for radially excited states.

At large n , the instanton-induced version does not keep with the expected Regge behavior $m_n^2 \sim n$. However, for experimentally observed (and usually discussed) bottomonia there is little practical difference between the potentials used. This is displayed in Fig. 5. Using the spin-averaged $1S$ states $\Upsilon(1S)$, η_b in input, we calculated masses of higher states for both potentials. As one can see, for $2S$ and $3S$ states the instanton-based potential gives masses *closer* to experiment than linear potential. Only by $4S$ do these deviations become of the same magnitude (but opposite sign), and for still higher states the linear potential is presumably better. The message from this plot is that, unless one goes beyond the $4S$ shell—to very large distances—both potentials predict masses with comparable accuracy.

B. Contributions to V_C of $I\bar{I}$ molecules

We start with $I\bar{I}$ pairs, with a fixed distance R_μ between the centers. The contribution to the central potential strongly depends on the orientation of this vector. When it is lined in time direction, $R_\mu = (0, 0, 0, R)$, as shown in the left of Fig. 6, the electric field and potential $\vec{E}(x)$, $A_4(x)$ are time-odd, with the opposite sign between lower and

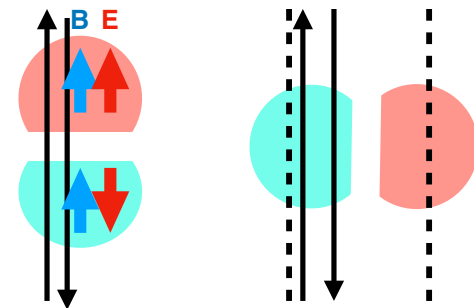


FIG. 6. Instanton–anti-instanton molecule oriented along the time axes (left) and space axes (right).

upper subvolumes, the instanton and anti-instanton. Therefore, the color rotation angles in the Wilson lines—integrated over time along the lines with arrows—get contributions of opposite sign which *cancel*. We thus come to the somewhat surprising conclusion that this configuration would *not* contribute to the central potential.

This is not so if R_μ has other orientations, e.g. in one of the space directions. Then the time-oriented Wilson lines would go through either the self-dual or anti-self-dual parts of the molecule. At small enough distance between both of them $r < \rho$ they are likely to go through the same duality, and therefore the result would be qualitatively the same as for a single instanton (discussed in the preceding subsection). At large $r \sim 2\rho$ the opposite would be dominant, with one of the angles in expression (18) changing sign.

C. Fixed energy tunneling events and their contribution to V_C

Tunneling in vacuum in a topological landscape proceeds at energy zero. But for quarks moving inside hadrons, or during some hadronic reactions, a certain amount of kinetic energy is available. Therefore tunneling through topological barriers may occur not via a BPST instanton but with modified tunneling solution, at some nonzero energy. These paths were sketched in the right side of Fig. 3: they include two Minkowskian sections of the path and an Euclidean one. The analytic solutions for a family of such paths, of Yang-Mills equations, can be obtained.

Their Euclidean part interpolates between two “turning point” magnetic configurations. As a result, the change in Chern-Simons number is fractional. Depending on the energy, one can obtain a single-parameter family of solutions, which interpolate between the bottom of the topological barrier (instanton) and its top (the sphaleron configuration). When analytically continued to Minkowski signature they describe implosion and explosion to and from the magnetic turning points.

Step 1: In order to obtain such solutions, use the O(4) static and symmetric ansatz for the SU(2) configuration in regular gauge

$$A_M^a(y) = 2\bar{\eta}_{aMN} \frac{y_N}{y^2} f(\xi) \quad (22)$$

with the conformal variable $\xi(y) = \frac{1}{2} \ln(y^2/\rho^2)$. The passage to singular gauge follows from the substitution $f(\xi) \rightarrow f(\xi) - 1$. The corresponding gauge invariant action is

$$S_S = -\frac{1}{4} \int d^4y F_{MN}^a F_{MN}^a \quad (23)$$

or in terms of the conformal variable

$$S_S = 24\pi^2 \int d\xi \left(\frac{f'^2(\xi)}{2} + V(f(\xi)) \right) \quad (24)$$

with the inverted double well potential

$$-V(f) = -2f^2(1-f)^2$$

in Euclidean signature. The O(4) profile $f(\xi)$ extremizes (23) and solves the Jacobi equation

$$\frac{d^2 f}{d\xi^2} = 4(f^2 - f)(2f - 1). \quad (25)$$

The solution to (25) with a sphaleronlike turning point at $\xi = 0$ with zero momentum $f'(\xi = 0) = 0$ is

$$f_k(\xi) = \frac{1}{2} \left(1 + \left(\frac{2k^2}{1+k^2} \right)^{\frac{1}{2}} \operatorname{sn} \left(\xi \left(\frac{2}{1+k^2} \right)^{\frac{1}{2}} - K(k), k \right) \right) \quad (26)$$

with sn the Jacobi sine function. Equation (26) forms a k family of ξ -periodic functions with the period

$$T_k = 4K(k) \left(\frac{1+k^2}{2} \right)^{\frac{1}{2}} \quad (27)$$

with $K(k)$ the elliptic function.

The solution (26) carries energy (conjugate to ξ coordinate) at the turning point

$$E_k = \frac{24\pi^2}{\rho} V(f_k(\xi = 0)) = E_0 \left(\frac{1-k^2}{1+k^2} \right)^2 \quad (28)$$

with $E_0 = 3\pi^2/\rho$. Equation (28) interpolates continuously between the sphaleron and the instanton for $0 \leq k \leq 1$. At $k = 0$ the energy E_0 is maximal and corresponds to sphaleron mass, the period is $T_0 = \sqrt{2}\pi$, and the profile $f_0(\xi) = \frac{1}{2}$ is constant. At $k = 1$ the instanton energy is $E_1 = 0$, the period $T_1 = \infty$, and the profile is

$$f_1(\xi) = \frac{1}{2} + \frac{1}{2} \operatorname{sn}(\xi - K(1), 1) = \frac{e^{2(\xi-K(1))}}{1 + e^{2(\xi-K(1))}}. \quad (29)$$

Note that the argument shift with $K(1)$ in (29) amounts to a rescaling of the instanton size in the conformal coordinate $\rho \rightarrow \rho e^{K(1)}$.

In general, the solution (26) carries Chern-Simons number N_k as well, that is tied to the energy E_k through the profile of the potential

$$\left(\frac{E_k}{E_0} \right) = 16N_k^2(1 - N_k)^2 \quad (30)$$

with $N_{k=1} = 1$ the instanton topological charge, and $N_{k=0} = \frac{1}{2}$ the sphaleron Chern-Simons number. Only the solution with

$N_1 = 1$ is self-dual and stable. All the other sphaleronlike configurations with $N_k < 1$ are unstable extrema. The flavor analog of these configurations was recently used to construct stable holographic tetraquark states [49,50].

Step 2 is applying the conformal (stereographic) mapping of the previous solutions that projects the $O(4)$ turning points on the sphere at $\xi^2 = \rho^2$ onto the planar turning point at $t_E = 0$,

$$(x + a)_\mu = \frac{2\rho^2}{(y + a)^2} (y + a)_\mu \quad (31)$$

with $a_\mu = (0, 0, 0, \rho)$. As a result, the gauge fields depend separately on the Euclidean coordinates $t_E = x_4 - Z_4$ and $r = |\vec{x} - \vec{Z}|$ (and parametrically on k)

$$\begin{aligned} A_4^a(t_E, r; k) &= \left(\frac{8\rho t_E x_a}{[(t_E + \rho)^2 + r^2][(t_E - \rho)^2 + r^2]} \right) f_k(\xi_E), \\ A_i^a(t_E, r; k) &= \left(\frac{\delta_{ai}(-t_E^2 - r^2 + \rho^2) + 2\rho\epsilon_{aij}x_j + 2x_i x_a}{[(t_E + \rho)^2 + r^2][(t_E - \rho)^2 + r^2]} \right) 4\rho f_k(\xi_E), \end{aligned} \quad (32)$$

with $Z_\mu = (\vec{Z}, Z_4)$ the collective position, and

$$\xi_E = \frac{1}{2} \ln \left(\frac{(t_E + \rho)^2 + r^2}{(t_E - \rho)^2 + r^2} \right). \quad (33)$$

In Euclidean signature, A_4 and the electric field are real and vanishing at $t_E = 0$ as they should, while A_i and the magnetic field are finite and real. Similar configurations were originally discussed in [51,52]. The half-periodicity (27) maps onto the tunneling time ($r = 0$)

$$\mathcal{T}_k = \rho \left(\frac{e^{\frac{1}{2}\mathcal{T}_k} - 1}{e^{\frac{1}{2}\mathcal{T}_k} + 1} \right) = \rho \tanh \left(\frac{1}{4}\mathcal{T}_k \right) \leq \rho. \quad (34)$$

The conformal transforms of the electric and magnetic fields in (D1) are lengthy. The sphaleron configuration with $k = 0$ and $f_0 = \frac{1}{2}$ has $A_4 = 0$ at the turning point $t_E = 0$, with an $O(3)$ symmetric and well-localized squared magnetic field

$$\vec{B}^2(0, r; 0) = \frac{96\rho^4}{(\rho^2 + r^2)^4}. \quad (35)$$

$$W(r; k) = \exp \left(i \left[\int_{-\infty + iT_k}^{iT_k} dt \frac{1}{2} A_4^a(-it, r; k) \tau^a + \int_{iT_k}^0 dt \frac{1}{2} A_4^a(-it, r; k) \tau^a + \int_0^\infty dt \frac{1}{2} A_4^a(-it, r; k) \tau^a \right] \right). \quad (37)$$

At the sphaleron point with $f_{k=0} = 1/2$, we can check that $W(r; k = 0) = 1$ and no self-energy is generated in going through a finite energy tunneling configuration. This result follows by deforming the contour on the real axis, without

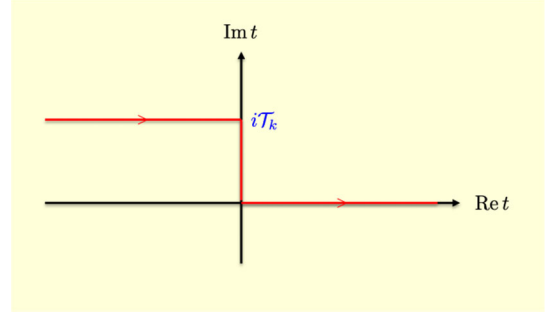


FIG. 7. Zigzag path for a temporal Wilson line describing a heavy quark traveling from one vacuum to another with a different topological charge, and riding a fixed energy tunneling configuration with tunneling time \mathcal{T}_k .

When analytically continued to Minkowski signature $t_E \rightarrow -it$, the gauge fields (32) describe a spherically outgoing (incoming) luminal thin shell, as the exiting sphaleron explodes (implodes) on its way downhill (uphill). The luminal shell supports only lightlike fields which are purely transverse, and fall off as $1/t$ at large times. It was previously used to describe “sphaleron explosion” in [28].

The fixed energy topological solutions contribute to Wilson lines, as a heavy quark travels from one vacuum to another vacuum with one added (subtracted) topological charge. In Minkowski signature, it corresponds to the zigzag path shown in Fig. 7,

$$\mathcal{C} = \cup] -\infty + iT_k, iT_k[\cup [iT_k, 0[\cup [0, +\infty[\quad (36)$$

where on the purely imaginary $[iT_k, 0]$ path, the heavy quark is riding the tunneling process. A similar path choice was also advocated for scattering processes through instantons in [53].

The chief contribution to the timelike Wilson line follows from this path, since the gauge field on the paths with real time support is luminal and transverse asymptotically,

encountering poles for $\mathcal{T}_{k=0} < \rho$, and noting that A_4 is time-odd. Away from the sphaleron point, a fraction of the instanton self-energy can be picked through the emergence of a complex singularities solution to $f_k(\xi) = \infty$.

III. SPIN-DEPENDENT POTENTIALS

A. Phenomenology, from heavy to light quarks

To start, let us consider the first $1S$ -shell, with zero orbital momentum $L = 0$, to recall the magnitude of the spin-spin forces. Starting from heavy quarkonia and proceeding to lighter systems, we focus on the following selection of mass splittings (all in MeV)

$$M(\Upsilon) - M(\eta_b) = 61; \quad (38)$$

$$\begin{aligned} M(J/\psi) - M(\eta_c) &= 116; & M(\psi^{2S}) - M(\eta_c^{2S}) &= 51; \\ M(B^*) - M(B) &= 35.5; & M(D^*) - M(D) &= 137; \\ M(K^*) - M(K) &= 398; & M(\rho) - M(\pi) &= 636. \end{aligned}$$

Note that these splittings grow for lighter quarks, eventually getting comparable to the scale of the mesonic masses: therefore in those cases spin forces cannot be treated as a perturbation.

Naively, the flavor dependence of the spin-spin forces should just follow from the product of the quark magnetic moment, which is $\sim 1/m_{Q_1}m_{Q_2}$, times some universal magnetic fields in the QCD vacuum as defined in the correlators of Appendix B. Yet the select splittings above show that that it is not the case even for heavy quarks: e.g. charm and bottom effects are different by a factor of 2, not 10 as the mass ratio would suggest. Yet universal vacuum correlators/potentials do not imply universal (mass-independent) matrix elements, since all of these mesons have vastly different wave functions. Especially interesting is the case of charmonium [second line in (38)] in which one has both the splittings of $1S$ and $2S$ levels. Not only the overall volume and $\psi(r=0)$ are different, but also the wave function of the $2S$ state has a node. The ratio of wave functions squared is shown in Fig. 8, and one can see that it changes from 0.538 at $r = 0$ to zero at $r \approx 2 \text{ GeV}^{-1}$. The ratio of the observed

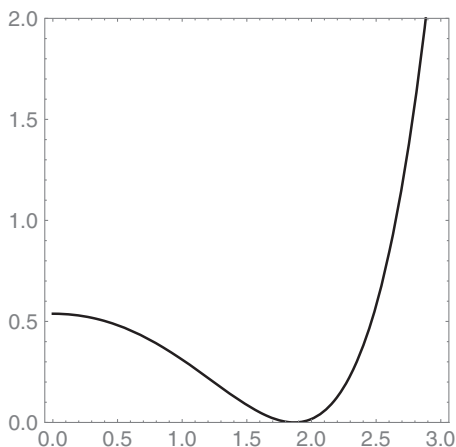


FIG. 8. The ratio of wave functions squared $\psi_{2S}(r)^2/\psi_{1S}(r)^2$ as a function of distance $r(\text{GeV}^{-1})$.

splittings is $51/113 \approx 0.45$ is comfortably in between, but much closer to the former number than to the latter one. This observation alone tells us that V_{SS} must be concentrated at very small distances.

Going further in phenomenology, we now proceed to the $1P$ shell, with $L = 1$. For any flavor combination, there are four states we will be interested in as above, starting from heavy quarkonia to heavy-light and all the way to mesons made of light quarks. For the light mesons we select two channels, the strange-light K mesons and charge $I = 1$ sector of the light-light. (The $I = 0$ sector has complicated mixing between quark states and glueballs, which we prefer not to include.) The results are listed in Table I. For example, the χ_{b2} state is the $\bar{b}b$ state with $S = 1$, $L = 1$, $J = 2$, and the h_b state has $S = 0$, $L = 1$, $J = 1$. All the names and masses are from the 2020 PDG tables.

With $L = 1$ all three spin-dependent terms come into play, and with four masses one has three differences which allow us to solve for each individual contribution. We define the differences from the χ to h states as

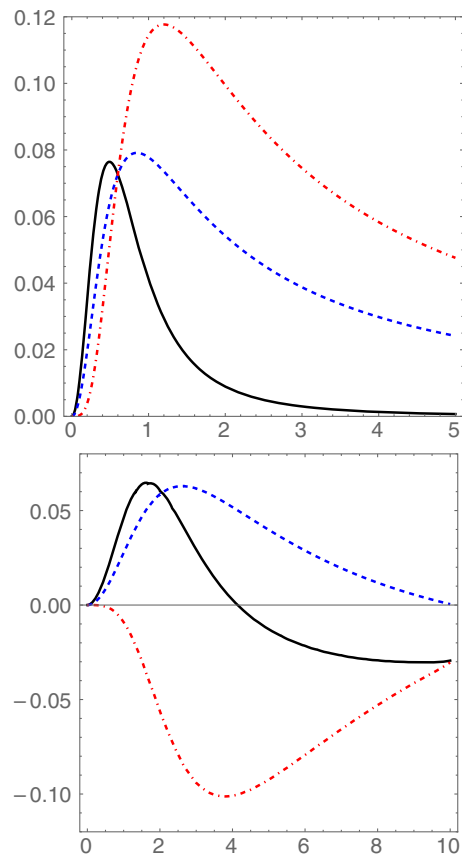


FIG. 9. Perturbative (top) and instanton-induced (bottom) spin-dependent potentials for charmonium. The black solid, blue dashed, and red dash-dotted lines are for $r^2 V_{SS}$, $r^2 V_{SL}$, $r^2 V_T$, in GeV^{-1} , versus r in GeV^{-1} .

TABLE I. The first column is the flavor composition. The next four columns refer to four states of the $n = 1$, P -shell with the quantum numbers explained in the text. The last three columns are matrix elements of spin-orbit, tensor, and spin-spin terms, in MeV.

	$S = 1, J = 2$	$S = 1, J = 1$	$S = 1, J = 0$	$S = 0, J = 1$	a	b	c
$\bar{b}b$	$\chi_{b2}(9912)$	$\chi_{b1}(9893)$	$\chi_{b0}(9859)$	$h_b(9899)$	13.7	3.3	0.5
$\bar{c}c$	$\chi_{c2}(3556)$	$\chi_{c1}(3511)$	$\chi_{c0}(3415)$	$h_c(3525)$	35	10	0.1
$\bar{c}q$	$D_2^*(2461)$	$D_1(2430)$	$D_0^*(2300)$	$D_1(2421)$	34	16	12
$\bar{s}q$	$K_2(1430)$	$K_1(1403)$	$K_0(1430)$	$h_s(1270)$	6.7	-5.6	151
$\bar{q}q$	$a_2(1317)$	$a_1(1230)$	$a_0(1450)$	$b_1(1235)$	0.5	-36	68

$$a\langle(\vec{S} \cdot \vec{L})\rangle + b\langle S_{12}\rangle + c\langle(\vec{S}_1 \cdot \vec{S}_2)\rangle.$$

We can solve for a , b , c by using the corresponding quantum numbers for these states, namely

$$\begin{aligned} M(\chi_{b2}) - M(h_b) &= a - (2/5)b + c, \\ M(\chi_{b1}) - M(h_b) &= -a + 2b + c, \\ M(\chi_{b0}) - M(h_b) &= -2a - 4b + c. \end{aligned} \quad (39)$$

The results are listed in the last three columns of Table I. The ensuing comments are as follows:

- (1) The spin-orbit matrix element a for heavy quarks is dominant.

- (2) The spin-orbit gets smaller for light quarks. Why?
- (3) The tensor force grows for heavy-light but then flips sign for light quarks. Why?
- (4) The spin-spin term grows and is dominant for light quarks.

We now proceed to see whether these observations can be explained by the theory we discuss below.

B. Wilson lines and the five potentials

Eichten and Feinberg [11] defined general spin-dependent interactions of heavy quarks in terms of *a priori* five potentials (see their definitions and further discussion in Appendix A) which contribute as follows:

$$\begin{aligned} V_{\text{SD}} &= \left(\frac{S_Q \cdot L_Q}{2m_Q^2} - \frac{S_{\bar{Q}} \cdot L_{\bar{Q}}}{2m_{\bar{Q}}^2} \right) \left(\frac{1}{r} \frac{d}{dr} (V_C(r) + 2V_1(r)) \right) \\ &+ \left(\frac{S_{\bar{Q}} \cdot L_Q}{m_Q m_{\bar{Q}}} - \frac{S_Q \cdot L_{\bar{Q}}}{m_{\bar{Q}} m_Q} \right) \left(\frac{1}{r} \frac{d}{dr} V_2(r) \right) + \frac{(3S_Q \cdot \hat{r} S_{\bar{Q}} \cdot \hat{r} - S_Q \cdot S_{\bar{Q}})}{3m_Q m_{\bar{Q}}} V_3(r) + \frac{1}{3} \frac{S_Q \cdot S_{\bar{Q}}}{m_Q m_{\bar{Q}}} V_4(r). \end{aligned} \quad (40)$$

$\vec{S}_{Q,\bar{Q}}$ and $\vec{L}_{Q,\bar{Q}}$ are the spin and orbital angular momenta of the $\bar{Q}Q$ pair. $V(r)$ is the central static potential, $V_1(r)$ and $V_2(r)$ are obtained by inserting a chromoelectric or chromomagnetic field on the temporal Wilson loop. The spin-spin and tensor contributions $V_{3,4}(r)$ follow from the insertion of two chromomagnetic fields on the Wilson loop. Equation (40) is exact to order $1/m_Q^2$. The last spin-spin part is fixed as $V_4(r) = 2\nabla^2 V_2(r)$ [11]. Lorentz invariance ties the central potential $V_C(r)$ to the spin-orbit potentials $V_{1,2}(r)$ through the so-called Gromes relation [54]

$$V_C(r) = V_2(r) - V_1(r). \quad (41)$$

The spin-dependent contributions emerging from the string were discussed by Buchmuller [55] and others [54,56]. Since the spin-spin interactions are short ranged, only the spin-orbit contributions survive at large separation b_\perp . This is manifest from (41) with $V_2(r) \rightarrow 0$ and $V_C(r) \rightarrow -V_1(r)$ asymptotically, hence [54–56]

$$\begin{aligned} V_{SL,\text{string}}(b_\perp) &= - \left(\frac{S_Q \cdot L_Q}{2m_Q^2} - \frac{S_{\bar{Q}} \cdot L_{\bar{Q}}}{2m_{\bar{Q}}^2} \right) \frac{\sigma_T}{b_\perp} \\ &\rightarrow - \frac{\sigma_T}{2m_Q^2 b_\perp} S \cdot L \end{aligned} \quad (42)$$

with $V_C(r) = \sigma_T r$, $\vec{S} = \vec{S}_Q + \vec{S}_{\bar{Q}}$ and $\vec{L} = \vec{L}_Q = -\vec{L}_{\bar{Q}}$. Since the electric flux tube is confined to the string, the spin-orbit contribution is only due to Thomas precession which is of opposite sign and half the spin-orbit contribution from the central potential. This can be understood from (40) to (41) if we assume that $V_2(r)$ is short range, so that $V_C(r) = -V_1(r)$. This string-induced spin-orbit effect is dubbed scalarlike in contrast to the Coulomb-induced spin-orbit effect which is vectorlike.

C. Lattice studies

The static spin-spin potentials have been evaluated on the lattice, using correlators of Wilson lines with explicit field strengths. In particular, Koma and Koma [57] find that while V_{SS} is indeed rather short range, it does not fit to

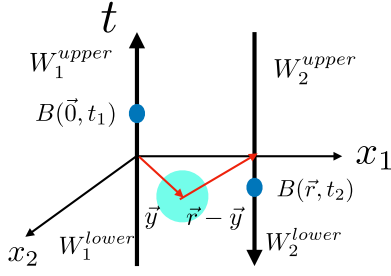


FIG. 10. Notations of vectors in evaluation of Wilson lines with two field strengths.

the vector + scalar exchange paradigm: a pseudoscalar glueball exchange has been proposed. Skipping a decade, Kawanai and Sasaki [58] accurately derived the central and spin-spin potentials for the $\bar{c}c$ and $\bar{s}s$ families, and used them in effective Schrödinger equations for a spectroscopic analysis with nice agreement with the spectroscopic data. In Fig. 12 we show (solid line) their exponential fit (for $\bar{c}c$),

$$V_{SS}^{\bar{c}c} \equiv \alpha e^{-\beta r}, \quad \alpha = 2.15 \text{ GeV}, \quad \beta = 2.93 \text{ GeV}. \quad (43)$$

Let us try to interpret this result: Naively, the coefficient in the exponent should be the mass of the object exchanged: for a gluon it should be about half of glueball masses, of the order of 1 GeV or so. It is in fact larger by a factor of 3. Why is it so large?

Fortunately, one can check it phenomenologically and find that it does describe well the $2S$ to $1S$ splitting in charmonium. Using this V_{SS} parametrization from [58] we calculate $1S$ triplet-singlet splitting to be 113.7 MeV (experimental value is 113 MeV) and $2S$ to be 47.3 MeV (experimental value is 51 MeV). While not perfect, this version of V_{SS} clearly does the job, at least in charmonium.

D. Spin-dependent forces from instantons

We decided first not to rely on general relations, sometimes leading to singular functions, and evaluated the correlators of Wilson lines with fields directly.

The notations we use for the evaluation of the spin-dependent potentials are shown in Fig. 10. The Wilson line W_1 is located at the origin of the spatial coordinates $\vec{0}$, and W_2 at $\vec{r} = (r, 0, 0)$. Two magnetic fields are inserted on them, and act at times t_1 and t_2 , respectively. The SU(2)

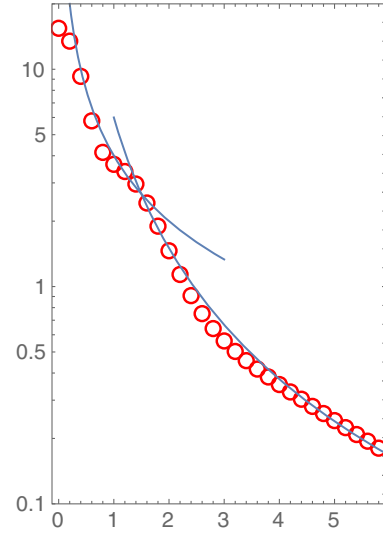


FIG. 11. The dependence of the integrated correlator of two magnetic fields (44) on the distance, in units of r/ρ , is shown by points. The two thin lines are drawn for comparison, the upper is $\sim 1/r$ and the lower $\sim 1/r^2$.

color matrix associated with the field B_m is τ^m , and the overall color trace defines the following tensor:

$$C^{m\bar{m}} = \text{Tr}[W_1^{\text{upper}}(W_2^{\text{upper}})^{\dagger} + \tau^{\bar{m}}(W_2^{\text{lower}})^{\dagger} + W_1^{\text{lower}}\tau^m].$$

This construction is implicitly included in what we denote by the “double average,” for example the spin-spin potential is related to the correlator of two magnetic fields integrated over their time difference

$$V_4(r) = \int dt \langle\langle B^{ma}(\vec{0}, 0) B^{ma}(\vec{r}, t) \rangle\rangle. \quad (44)$$

The center of the instanton is put at time zero and spatial location \vec{y} . On dimensional grounds, the instanton of size ρ should contribute to those potentials $\sim \kappa 1/\rho^3 F(r/\rho)$.

The field strength for an instanton (in regular gauge), located at point y , is

$$G_{\mu\nu}^a(x) = -4\eta_{\mu\nu}^a \frac{\rho^2}{((x-y)^2 + \rho^2)^2}. \quad (45)$$

Four Wilson lines are written in their canonical form $W = \cos(A) + i(\vec{n} \cdot \vec{\tau}) \sin(A)$ with certain angles, which in regular gauge are

$$\begin{aligned} A_1^{\text{lower}} &= -\left[\pi + 2 \arctan\left(\frac{t_1}{\sqrt{y^2 + \rho^2}}\right) \right] \frac{1}{\sqrt{1 + \rho^2/y^2}}, \\ A_2^{\text{lower}} &= -\left[\pi + 2 \arctan\left(\frac{t_2}{\sqrt{r^2 + y^2 - 2ry \cos(\theta) + \rho^2}}\right) \right] \frac{1}{\sqrt{1 + \rho^2/(r^2 + y^2 - 2ry \cos(\theta))}}. \end{aligned} \quad (46)$$

The “upper” lines are given by the same expressions with opposite signs of \arctan . If there are no field insertions, these terms cancel as they should, and their sum becomes the angles we already met in the expression for central potentials.

In total, the correlator includes integration over d^3y, t_1, t_2 . With the azimuthal angle ϕ_y being irrelevant, it is a four-dimensional integral performed numerically. The results are shown in Fig. 11. In this log plot one can see that the resulting spin-spin force rapidly decreases with

distance. For comparison, we show two lines with $1/r$ and $1/r^2$, which approximately reproduces the behavior. One should not however conclude that they give a correct analytic asymptotic: in fact, expanding the integrand in inverse powers of r leads to divergences of the remaining integrals, indicating that the true asymptotic behavior cannot be just powers.

In the instanton vacuum, with (anti-)self-dual fields $\vec{E}^a = \pm \vec{B}^a$ in Euclidean signature, all potentials in (40) can be tied to the central potential $V_C(r)$ [10,11,47]

$$V_C(r) + 2V_1(r) \rightarrow 0, \quad V_2(r) \rightarrow \frac{1}{2}V_C(r), \quad V_3(r) \rightarrow -\left(\frac{1}{r}V_C' - V_C''\right) \quad (47)$$

and the simplified spin-orbit contribution

$$\left[\frac{1}{2m_Q^2} \frac{1}{r} \frac{d}{dr} V_C(r)\right] (S_Q + S_{\bar{Q}}) \cdot L_Q \equiv \left[\frac{1}{2m_Q^2} \frac{1}{r} \frac{d}{dr} V_C(r)\right] S \cdot L. \quad (48)$$

Schematically, the central electric interaction $\langle E_i^a(x) \times [x, 0]^{ab} E_i^b(0) \rangle$ is amenable to the spin-orbit interaction $\langle E_i^a(x) [x, 0]^{ab} B_i^b(0) \rangle$ and also the spin-spin and tensor interaction $\langle B_i^a(x) [x, 0]^{ab} B_i^b(0) \rangle$.

In Fig. 12 we compare the perturbative (dashed-dotted black line) and nonperturbative (dashed blue line) spin-spin potentials with the lattice result (solid black line). Recall that the Laplacian of the Coulomb force is a delta function, well known in atomic and positronium physics. However, one should use Coulomb potential $1/r$ in some

regulated form, for several reasons. First, when the potential gets as deep as (minus) mass, the nonrelativistic approximation itself should break down, so the spread cannot be smaller than $O(1/m_Q)$. Second, lattice studies include nonlocality in the form of the lattice spacing a . Third, a Gaussian-smeared delta function is actually used in many spectroscopic calculations, see e.g. [59]. For the perturbative spin-spin interaction, we use a simpler version, as the Laplacian of a Coulomb contribution regulated by a fixed parameter $\delta = 0.6 \text{ GeV}^{-1}$

$$V_{SS}^C(r) = -\frac{A}{3m_Q m_{\bar{Q}}} \vec{\nabla}^2 \frac{1}{\sqrt{r^2 + \delta^2}}. \quad (49)$$

For the nonperturbative spin-spin part, we use the instanton contribution, which is given by the Laplacian acting on the central potential

$$V_{SS}^{\text{inst}}(r) = \frac{1}{3m_Q m_{\bar{Q}}} \vec{\nabla}^2 V_C^{\text{inst}}(r). \quad (50)$$

All the potentials shown are multiplied by r^2 , as they appear in the volume integrals. So, if the wave functions are roughly constant at this small scale, the area under the curves in Fig. 12 gives an estimate of the relative contributions. So, one finds that the perturbative and nonperturbative parts contribute *comparably* to the total spin-spin potential, in sum roughly reproducing the lattice-based result. This observation is among the main findings of this work.

Of course, the actual magnitude of the spin splittings depends on the quark masses involved, explicitly via $1/m_Q^2$

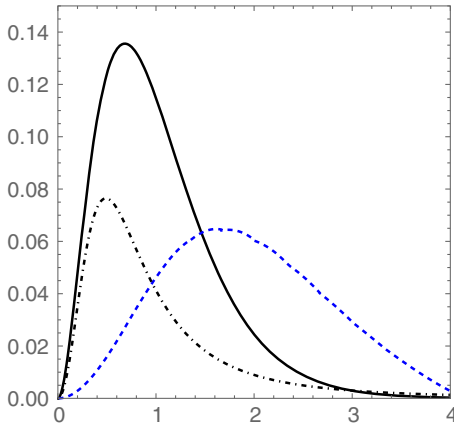


FIG. 12. Spin-spin potential for $\bar{c}c$ system multiplied by distance squared $r^2 V_{SS} (\text{GeV}^{-1})$ versus $r (\text{GeV}^{-1})$. The solid line is the exponential fit (43) to lattice measurements [58]. The dash-dotted line shows the regulated Laplacian of the Coulomb potential (49) with $\delta = 0.6 \text{ GeV}^{-1}$. The blue dashed line shows the instanton contribution. Note that the area under the last two curves is roughly equal to that under the solid one, the lattice fit.

TABLE II. “Hyperfine” splittings of certain $L = 0$ mesons with $J = 1$ and $J = 0$. The first row of numbers shows the experimental values (MeV) (rounded to 1 MeV). The second row gives the matrix elements of the lattice-based spin-spin potential (43), the next two rows are the (regulated) Coulomb and instanton-induced spin-spin contributions.

Flavors	$M_{\Upsilon} - M_{\eta_b}$	$M_{J/\psi} - M_{\eta_c}$	$M(D^*) - M(D)$	$M(K^*) - M(K)$	$M(\rho) - M(\pi)$
Experiment	61	116	137	398	636
$\langle V_{SS}^{\text{lat}}/3m_Q m_{\bar{Q}} \rangle$	46	108	98	170	
$\langle \vec{\nabla}^2 V_C/3m_Q m_{\bar{Q}} \rangle$	28	58	48	82	
$\langle \vec{\nabla}^2 V_{\text{inst}}/3m_Q m_{\bar{Q}} \rangle$	7	30	48	90	

factors and implicitly, via the wave functions. Lighter quarks lead generally to hadrons of larger size, or smaller wave functions at small distances.

The matrix elements of all three potentials shown in Fig. 12 were evaluated using wave functions from the Cornell potential irrespective of flavor. The results for the spin-spin contributions are in Table II. The results show that perturbative and nonperturbative contributions for heavy quarkonia do reproduce the splittings if *taken together*. Already for heavy-light mesons one can see that some additional effect seems to be missing; it will indeed as will be explained below. Furthermore, for the mesons containing only light quarks, both contributions together definitely fail to describe large splittings seen experimentally. Clearly some other effects are in play here, to be discussed below.

We continue our phenomenological description of the spin-dependent interactions, by considering the next four states in the 1P shell, with the onset of the spin-orbit and tensor potentials. The empirical information to be used on several mesonic families is listed in Table III. The theoretical estimates follow from 1P wave functions derived with standard Cornell potential. For both components of the central potential—perturbative and instanton-induced—we calculated the matrix elements of the three spin-dependent potentials using the formulas given above, and then calculated their matrix elements in the 1P shell.

One observation from this table is that the “theory” (the sum of the last two rows) and the lattice-induced one (the second row) are basically in agreement. The other is that their disagreement with experiment (the upper row) is dramatically growing for light quark systems. This implies that for light quarks something important is missed in the description as developed so far.

E. Contributions of $\vec{I}\vec{I}$ molecules to spin forces

Like in Sec. II B, let us start with the $\vec{I}\vec{I}$ molecules oriented in the time direction, for which $\vec{E} \sim G_{4m}$ and A_4 are time-odd. Therefore, as we noted before, there is no contribution to the central potential.

Yet the spin-spin and tensor forces are not at all zero, as the main contributors to the correlator come from the *magnetic* fields \vec{B} , which have *the same sign* in the I and \bar{I} parts of the molecule.

A detailed description of the $\vec{I}\vec{I}$ configuration can be achieved by the Yung ansatz, which is quite accurate. The corresponding expressions for field strengths were obtained in *Mathematica*, which are way too complicated to be given here. Yet the field strengths are approximately additive, and this approximation will be used in what follows.

Let us start with the correlator of two magnetic fields, measured at integrated times t_1 and t_2 on two temporal lines separated by a spatial distance r ,

TABLE III. Groups of three matrix elements of spin-spin, spin-orbit, and tensor potentials V_{SS}, V_{SL}, V_T , respectively. The first one in each group is the observed “exp” value from Table I; the second and the third values are the perturbative (pert) and instanton-induced contributions, corresponding to the Coulomb and instanton-induced (inst) parts of the central potential.

	SS “exp”	SS pert	SS inst	SL “exp”	SL pert	SL inst	T “exp”	T pert	T inst
$\bar{c}c$	0.1	0.56	1.9	35	3.2	3.8	10	5.8	-5.7
$\bar{s}q$	151	5	29	6.7	31	38	-5.6	58	-46
$\bar{q}q$	68	8	48	0.5	52	64	-36	96	-78

$$\begin{aligned}
\int dt \langle B^{ma}(0, \vec{0}) B^{ma}(t, \vec{0}) \rangle &= \int dt_1 dt_2 d^3y (48n_{\text{mol}}\rho^4) \\
&\times \left(\frac{1}{((t_1 - R/2)^2 + \rho^2 + y^2)^2} + \frac{1}{((t_1 + R/2)^2 + \rho^2 + y^2)^2} \right) \\
&\times \left(\frac{1}{((t_2 - R/2)^2 + \rho^2 + y_2^2)^2} + \frac{1}{((t_2 + R/2)^2 + \rho^2 + y_2^2)^2} \right). \quad (51)
\end{aligned}$$

Here y^2 and $y_2^2 = y^2 + r^2 - 2ry \cos(\theta_{ry})$ are the squared 3d distances to the first and second Wilson lines. We assumed additivity of the magnetic fields from I and \bar{I} , and ignored the color rotation angles on the Wilson lines (which vanish at the instanton center, as we already know).

At zero distance between the line $r = 0$, all integrations can be done analytically, with the result

$$\int dt \langle B_1^{ma}(0, \vec{0}) B_2^{ma}(t, \vec{0}) \rangle_{r=0} = 12\pi^4 \rho n_{\text{mol}}. \quad (52)$$

For qualitative orientation, one can compare this expression to (the extrapolation of) the lattice spin-spin potential (43) to $r = 0$; they are equal if $n_{\text{mol}} \approx 7 \text{ fm}^{-4}$.

Note that in this approximation there is no dependence on the (time) separation R of I and \bar{I} centers. For nonzero r the volume integral over y , $\cos(\theta_{ry})$ is done numerically; see the results in Fig. 13.

Now let us calculate the same correlator, but for a molecule rotated so that its vector R_μ joining the centers, lines in the spatial direction, say the same as the vector \vec{r} between the Wilson lines. The electric and certain magnetic fields exchange places and the expression changes into

$$\begin{aligned}
\int dt \langle B^{am}(0, \vec{0}) \vec{B}^{am}(t, \vec{0}) \rangle &= \int dt_1 dt_2 dy_1 2\pi y_\perp dy_\perp (48n_{\text{mol}}\rho^4) \\
&\times \left(\frac{1}{(t_1^2 + \rho^2 + (y_1 - R/2)^2 + y_\perp^2)^2} - \frac{1}{(t_1^2 + (y_1 + R/2)^2 + \rho^2 + y_\perp^2)^2} \right) \\
&\times \left(\frac{1}{(t_2^2 + \rho^2 + (y_1 - R/2 + r)^2 + y_\perp^2)^2} - \frac{1}{(t_2^2 + (y_1 + R/2 + r)^2 + \rho^2 + y_\perp^2)^2} \right). \quad (53)
\end{aligned}$$

In Fig. 13 we compare the correlators for two molecule orientations with averaging factors, $(1/4)$ (51) and $(3/4)$ (53) by upper and lower points, as well as their sum (the line). So, while the two contributions have different dependence on r , the orientation-average $V_{SS}(r)$ decreases monotonously, and has the effective width (at half maximum) close to the average instanton size ρ . Note that this range is shorter than $V_{SS}(r)$ from the instantons alone (calculated from the Laplacian of the contribution to the central potential in the previous subsection), and it does not have a negative part. It is therefore closer in shape to what was found on the lattice.

The *spin-orbit* force is qualitatively different from spin-spin ones, being related to a correlator $\int dt \vec{E} \vec{B}$. For a time-oriented molecule $R_\mu = (0, 0, 0, R)$ $\vec{E}(t)$ is time-odd and $\vec{B}(t)$ is time-even, so for this molecule orientation this correlator vanishes. The situation is different for a space-oriented molecule, say along x_1 . Now G_{1m} , $m = 2, 3, 4$ fields are odd in x_1 inversion, but everything is even along the time axes. The expression for the correlator can easily be constructed and calculated in a way similar to what was done above for $V_{SS}(r)$.

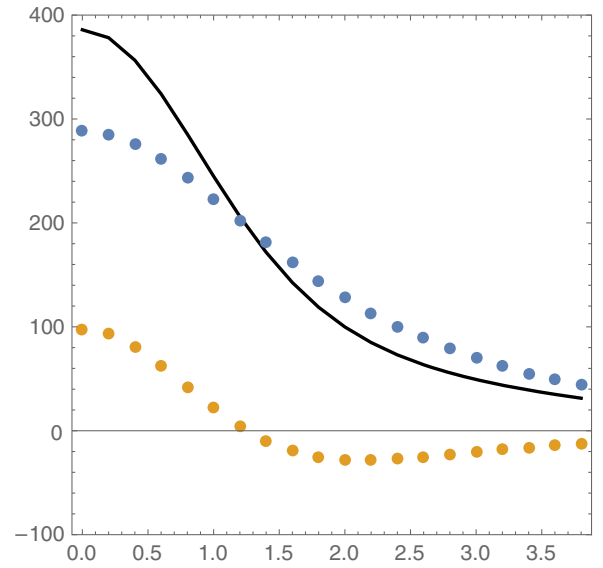


FIG. 13. The normalized correlators $(1/4)$ (51) (upper points) and $(3/4)$ (53) for $R = \rho$ (lower points) in units of $n_{\text{mol}}\rho$, versus the distance between the Wilson lines r/ρ . The solid line shows their sum.

We conclude that the ‘‘molecule-induced’’ spin forces are quite similar to the instanton induced ones (apart from, of course, normalization to quite different densities) at small distances, but are *significantly reduced* at $r > 2\rho$ due to the partial cancellations by different orientations.

In the previous section we have seen that, in the approximation of molecules represented as two independent pseudoparticles, the nonperturbative $V_{SS(r)}$ have about the right magnitude, but somewhat too large range. We now see that a better description of the field structure has the potential to remedy this problem.

F. Contributions of the fixed energy tunneling configurations to spin forces

The finite energy tunneling configurations contribute to the spin forces, through close Wilson loops dressed by E, B fields. However, since these configurations cease to be self-dual for $0 \leq k < 1$, the induced spin potentials are in general independent. Moreover, these configurations carry t-odd electric fields, and are purely magnetic at the exit points ($t_E = 0$). They may only contribute to the spin-spin and tensor potentials.

The explicit expression of the magnetic field in Euclidean time is

$$\begin{aligned} B^{ma}(t_E, \vec{x}) = & \delta^{ma} \left(-\frac{16\rho^2}{\mathbb{D}} f + \frac{8\rho^2 r^2}{\mathbb{D}^2} fF + \frac{32\rho^3 t_E r^2}{\mathbb{D}^2} f' + \frac{32r^2 \rho^2}{\mathbb{D}^2} f^2 \bar{F} \right) \\ & + x^m x^a \left(-\frac{8\rho^2}{\mathbb{D}^2} fF - \frac{32t_E \rho^3}{\mathbb{D}^2} f' + \frac{32\rho^2}{\mathbb{D}^2} f^2 F \right) \\ & + \epsilon^{mai} x^i \left(\frac{16\rho}{\mathbb{D}} f + \frac{4\rho}{\mathbb{D}^2} fF \bar{F} + \frac{16t_E \rho^2}{\mathbb{D}^2} f' \bar{F} - \frac{32\rho^3}{\mathbb{D}^2} (2r^2 + \bar{F}) f^2 \right) \end{aligned} \quad (54)$$

with $f' = \partial_{\xi} f_k(\xi)$,

$$\mathbb{D} = (t_E^2 + r^2 + \rho^2)^2 - 4t_E^2 \rho^2 \quad (55)$$

and

$$F = t_E^2 + r^2 + \rho^2, \quad \bar{F} = -t_E^2 - r^2 + \rho^2. \quad (56)$$

The magnetic field in Minkowski signature follows from the substitution $t_E \rightarrow -it$.

The induced spin-spin interaction follows from the complexified path in the t plane shown in Fig. 7. An estimate of the magnitude of the spin-spin interaction, follows from zero separation between a path \mathcal{C} and $\bar{\mathcal{C}}$

$$\int_{\mathcal{C}} dt \int_{\bar{\mathcal{C}}} d\bar{t} \langle B^{ma}(-it, \vec{0}) B^{ma}(-i\bar{t}, \vec{0}) \rangle = [3 \cdot 2^8 \rho^4 n_k] \int_{\mathcal{C}} dt \int_{\bar{\mathcal{C}}} d\bar{t} \int d^4 Z \left(\frac{f \bar{f}}{\mathbb{D} \bar{\mathbb{D}}} \right) \quad (57)$$

with now

$$\begin{aligned} \mathbb{D} & \rightarrow ((-it - Z_4)^2 + \vec{Z}^2 + \rho^2)^2 - 4(-it - Z_4)^2 \rho^2, \\ \bar{\mathbb{D}} & \rightarrow ((-i\bar{t} - Z_4)^2 + \vec{Z}^2 + \rho^2)^2 - 4(-i\bar{t} - Z_4)^2 \rho^2, \end{aligned} \quad (58)$$

and $F = f_k(\xi)$ and $\bar{F} = f_k(\bar{\xi})$ with

$$\begin{aligned} \xi & \rightarrow \frac{1}{2} \ln \left(\frac{(-it - Z_4 + \rho)^2 + \vec{Z}^2}{(-it - Z_4 - \rho)^2 + \vec{Z}^2} \right), \\ \bar{\xi} & \rightarrow \frac{1}{2} \ln \left(\frac{(-i\bar{t} - Z_4 + \rho)^2 + \vec{Z}^2}{(-i\bar{t} - Z_4 - \rho)^2 + \vec{Z}^2} \right), \end{aligned} \quad (59)$$

with the Euclidean-Minkowski time assignments in (36).

At the sphaleron point $f_{k=0} = 1/2$, and (57) reduces to

$$\begin{aligned} \int_{\mathcal{C}} dt \int_{\bar{\mathcal{C}}} d\bar{t} \langle B^{ma}(-it, \vec{0}) B^{ma}(-i\bar{t}, \vec{0}) \rangle & \rightarrow [192 \rho^4 n_{k=0}] \int_{\mathcal{C}} dt \int_{\bar{\mathcal{C}}} d\bar{t} \int d^4 Z \\ & \times \frac{1}{(((-it - Z_4)^2 + \vec{Z}^2 + \rho^2)^2 - 4(-it - Z_4)^2 \rho^2) (((-i\bar{t} - Z_4)^2 + \vec{Z}^2 + \rho^2)^2 - 4(-i\bar{t} - Z_4)^2 \rho^2)}. \end{aligned} \quad (60)$$

Overall time translational invariance allows us to set $Z_4 = 0$ in the integrand, with the final result

$$\frac{\int_{\mathcal{C}} dt \int_{\bar{\mathcal{C}}} d\bar{t} \langle B^{ma}(t, \vec{0}) B^{ma}(\bar{t}, \vec{0}) \rangle}{\int dZ_4} = \frac{\pi^4}{4\rho^3}. \quad (61)$$

This result follows by deforming the complexified path to the real axis, without encountering poles for $T_{k=0} < \rho$. The spin-spin interaction (61), stemming from the finite energy tunneling configurations, is comparable to the spin-spin interaction (52) from the thimbles. At the sphaleron point and for zero separation, they are comparable when

$$\frac{n_{k=0}}{n_{\text{mol}}} = \frac{12\pi^4}{192\pi^4/4} = \frac{1}{4}. \quad (62)$$

IV. INTERQUARK FORCES INDUCED BY INSTANTON ZERO MODES ('T HOOFT EFFECTIVE LAGRANGIAN)

A. Pseudoscalar mesons which are and are not the Nambu-Goldstone modes

It has been known since the 1970s that in the chiral limit light-quark pseudoscalar mesons consist of octet π , K , η Nambu-Goldstone modes and a singlet η' which does *not* belong to that set, and is instead very heavy. It happens because the 't Hooft effective Lagrangian violates $U_A(1)$ and quite effectively generates flavor-changing annihilation processes

$$\bar{u}u \leftrightarrow \bar{d}d \leftrightarrow \bar{s}s.$$

When a strange quark mass is added, one finds $\eta - \eta'$ mixing which describes well the phenomenology of their decays. It sharply contrasts with the vector counterparts, ρ , ω , ϕ mesons, for which the mixing is very small.

To avoid these annihilation processes, one can discuss ‘‘flavored’’ channels, like $\pi^+ = \bar{d}u$, in which case the 't Hooft effective Lagrangian acts as a force between the quark and antiquark. Yet it is still different from the conventional forces we so far discussed, in that it exists for quarks of *different flavors* only. In Fig. 1 we illustrate how the 't Hooft induced vertex operates in the pion and rho charged meson channels.

Before we turn to specifics, let us comment on some lattice implementations of theories with different quarks. The simplest case is a single quark flavor theory, $N_f = 1$. In it the 't Hooft action is a 2-fermion operator: it gives the quark an effective mass but does not generate annihilations or interactions as we noted. The only pseudoscalar mesons is the analog of η' ; no π , K , η modes exist.

In lattice implementations nowadays one uses gauge ensemble for physical QCD, but still uses certain diagram and mass selections aiming to study certain unphysical particles. For example, in [60], an artificial particle called η_s

made of $\bar{s}s$ was introduced, with no mixing to other flavors. Its properties are deduced from the *connected* diagram, without the disconnected one in which the flavor is changed. One may explain its absence by introducing an *extra* valence quark species s' , and view source/sink operators as flavor-nondiagonal $\bar{s}s'$. Our comment is that such setting, while eliminating the annihilations, still keeps the 't Hooft effective Lagrangian producing a force between the quark and antiquark, as they are not of the same flavor. Apart from the mass values, this channel is no different from say $\pi^+ = \bar{d}u$ we consider.

In our first take on spin-spin forces in (38) we already observed anomalously large splitting between the ρ , $S = 1$ and π , $S = 0$ states in the lowest light quark shell, and have seen that the magnitude of $V_{SS}(r)$ discussed so far, is not sufficient to explain it. [In particular, adding $V_{SS}(r)$ as detailed above to the basic quark model, with the Cornell potential and a light quark constituent mass of 0.35 GeV, reduces the ground state $1S$ mass substantially, from 1.4 GeV to about 0.85 GeV. Yet it is still far from the observed pion mass of 0.138 GeV and from zero, which it should be in the chiral limit.]

Of course, a correct pion mass can only be explained in an approach, consistently explaining chiral symmetry breaking, as well as other parameters of chiral perturbation theory. Two famous models—NJL and ILM—are well-known examples of that.

Before we focus on the theory, let us return for a brief moment to the phenomenological constituent quark model, to see what kind of interaction one needs to add in order to obtain the experimentally observed pions. Let us assume that there is an additional interaction, that operates *only* between quarks of different flavors, on top of the flavor-blind forces so far discussed. Note that the usual discussion of $\pi - \eta'$ splitting is based on ‘‘annihilation channels’’ (like $\bar{u}u \leftrightarrow \bar{d}d$) as we continue to consider only charged mesons, like $\bar{d}u$.

The 't Hooft Lagrangian is usually written as a local operator *a la* NJL one, corresponding to a potential of the type $G_{\text{Hooft}} \delta^3(\vec{r})$ potential. This form assumes that the instanton size ρ is much smaller than the hadronic sizes, as it appears in the standard LSZ ‘‘amputation’’ of external propagator lines. Unfortunately, in the Euclidean setting of the instanton calculus, taking these lines on-shell amounts to the limit $p^\mu \rightarrow 0$ for all components. And yet, it is clear that the process is nonlocal, and that the scale of its size is ρ . Thus in model applications one includes form factors, usually the Fourier transform of the zero modes. We will use another ‘‘regulated delta function’’ form described in Appendix C.

Note: When the nonlocality induced by the parameter ρ is small compared to the hadron size, it can be well approximated by a delta function. However, this is not true for pions. This can be seen from the pion wave function (with or without the effective 't Hooft term): its

$r^2\psi_\pi^2(r)$ peaks at $r \approx \rho$ in this case. Therefore, in the pion case there remains certain dependence on a choice of the nonlocal approximation.

Finally, the coupling strength for the 't Hooft effective interaction to add to the discussed potentials above needed to reproduce the physical pion mass is found to be

$$G_{\text{Hooft}} \approx 17 \text{ GeV}^{-2}. \quad (63)$$

B. Chiral anomaly and instanton zero modes

It was well understood already in the 1970s that instantons provide an example of explicit violation of the $U_A(1)$ chiral symmetry. The divergence of the corresponding axial current is proportional to the topological charge density $G\tilde{G}$, which in turn is a divergence of the topological Chern-Simons current. Thus the axial charge of fermions, or the number of right minus left-polarized quarks, is intimately related to gauge topology.

How this happens in the instanton case was explained by 't Hooft [23], who found the existence of a four-dimensional bound state, or the *fermion zero mode* of the Dirac operator in the instanton background. Formally it amounts to an additional term in the four-dimensional quark propagator

$$S(x, y) = \sum_\lambda \frac{\psi_\lambda(x)\psi_\lambda(y)^+}{\lambda + im} \quad (64)$$

with the zero mode $\lambda = 0$. The physical meaning is that the negative energy Dirac sea creates a new state, into which the original quark is pushed into. At the same time, a quark

of *opposite chirality* emerges from the Dirac sea as a physical (positive energy) state.

This process can be described by a ‘‘chirality flip’’ of a quark. However, the phenomenon is not reduced just to this: *all* light quark flavors must experience this together and flip their chiralities *simultaneously*. Because of the Pauli principle, only the zero modes with different flavors can undergo simultaneous tunneling, the 't Hooft effective Lagrangian is therefore a six-quark operator, with $\bar{u}u\bar{d}d\bar{s}s$ quarks. As emphasized by 't Hooft, it is repulsive in the η' channel, and solves the famous $U_A(1)$ problem. But the fact that it is *attractive* in the scalar σ and pseudoscalar π, K, η octet channels leads to even more important consequences, breaking the $SU(N_f)$ chiral symmetry spontaneously [24]. The account for these effects led to the statistical studies of instanton ensembles in the 1990s, for a review see [12]. Many more studies based on these observations were carried in the last two decades as well; let us just mention our recent study of the so-called instanton-sphaleron production process, which can be studied experimentally in colliders [40].

For clarity, let us now discuss some technical issues already discussed in the literature. The first is the explicit analytic form of the 't Hooft operator, which, by Fierz transformations, can take several different forms. A straightforward reduction of the product of six unitary color rotation matrices, averaged over the $SU(3)$ group, leads to color structures containing $f^{abc}\lambda^a\lambda^b\lambda^c$ and $d^{abc}\lambda^a\lambda^b\lambda^c$ terms, which is difficult to use in practice. However they (and in fact all color matrices) can be eliminated using specific properties of zero modes producing the following result [61]:

$$\begin{aligned} \mathcal{V}_{qqq}^{L+R} = & \frac{G_{\text{Hooft}}}{N_c(N_c^2 - 1)} \left[\left(\frac{2N_c + 1}{2(N_c + 2)} \right) \left\| \begin{array}{ccc} \bar{u}_R u_L & \bar{u}_R d_L & \bar{u}_R s_L \\ \bar{d}_R u_L & \bar{d}_R d_L & \bar{d}_R s_L \\ \bar{s}_R u_L & \bar{s}_R d_L & \bar{s}_R s_L \end{array} \right\| \right. \\ & - \frac{1}{2(N_c + 1)} \sum_{a=1}^3 \left(\left\| \begin{array}{ccc} \bar{u}_R \sigma^a u_L & \bar{u}_R \sigma^a d_L & \bar{u}_R \sigma^a s_L \\ \bar{d}_R \sigma^a u_L & \bar{d}_R \sigma^a d_L & \bar{d}_R \sigma^a s_L \\ \bar{s}_R u_L & \bar{s}_R d_L & \bar{s}_R s_L \end{array} \right\| + \left\| \begin{array}{ccc} \bar{u}_R \sigma^a u_L & \bar{u}_R d_L & \bar{u}_R \sigma^a s_L \\ \bar{d}_R u_L & \bar{d}_R d_L & \bar{d}_R s_L \\ \bar{s}_R \sigma^a u_L & \bar{s}_R d_L & \bar{s}_R \sigma^a s_L \end{array} \right\| + \left\| \begin{array}{ccc} \bar{u}_R u_L & \bar{u}_R d_L & \bar{u}_R s_L \\ \bar{d}_R u_L & \bar{d}_R \sigma^a d_L & \bar{d}_R \sigma^a s_L \\ \bar{s}_R u_L & \bar{s}_R \sigma^a d_L & \bar{s}_R \sigma^a s_L \end{array} \right\| \right) \left. \right] \\ & + (L \leftrightarrow R) \end{aligned} \quad (65)$$

with the strength of the six-quark operator

$$G_{\text{Hooft}} = \frac{n_{I+\bar{I}}}{2} (4\pi^2 \rho^3)^3 \left(\frac{1}{m_u^* \rho} \right) \left(\frac{1}{m_d^* \rho} \right) \left(\frac{1}{m_s^* \rho} \right) \quad (66)$$

with the effective quark masses m_q^* to be explained a bit later.

In (65) all quarks and antiquarks have opposite chiralities. In a completely massless theory we cannot have ‘‘loop’’

quarks by a propagator conserving chirality. However, the spontaneous breaking of chiral symmetry in the QCD vacuum leads to nonzero quark condensates $\langle \bar{q}_f q_f \rangle \neq 0$. This fact leads to ‘‘dimensional reduction’’ of the six-quark operator to four- (and even two-) quark expressions, by ‘‘looping’’ some quark-antiquark pairs into the corresponding condensates. For example, strange quark loops generate an effective ud interaction. It also has a structure of two-by-two determinants, which (with some abuse of notations) we write as

$$\mathcal{V}_{qq}^{L+R} = \kappa_2 A_{2N} (\det(UD) + B_{2N} \det(U_{\mu\nu} D_{\mu\nu})) + (L \leftrightarrow R) \quad (67)$$

with

$$A_{2N} = \frac{(2N_c - 1)}{2N_c(N_c^2 - 1)}, \quad B_{2N} = \frac{1}{4(2N_c - 1)}. \quad (68)$$

The coefficient

$$\kappa_2 = 3! G_{\text{Hooft}} \langle \bar{s}_R s_L \rangle = 3 G_{\text{Hooft}} \langle \bar{s} s \rangle < 0$$

is negative and thus attractive. In the Weyl basis, $\sigma_{\mu\nu} \rightarrow i\eta_{\mu\nu}^a \sigma^a$ with the 't Hooft symbol satisfying $\eta_{\mu\nu}^a \eta_{\mu\nu}^b = 4\delta^{ab}$, and (67) can be simplified further

$$\mathcal{V}_{qq}^{L+R} = \kappa_2 A_{2N} (\det(UD) - 4B_{2N} \det(U^a D^a)) + (L \leftrightarrow R). \quad (69)$$

Another possible “looping” of quarks is possible if we account for nonzero quark masses, in particular the largest strange quark mass m_s . As a result, the effective ud interaction (containing the m_s term) is *stronger* than us, ds interactions, as they only contain negligibly small light quark masses. As noticed by one of us and Rosner [62], the ratio of the coefficients for light-light and light-strange four-fermion terms is

$$\frac{G(\bar{u}u\bar{d}d)}{G(\bar{u}u\bar{s}s)} = \frac{m_q^* + m_s}{m_q^*} \approx 1.5. \quad (70)$$

One consequence of this is the relatively large violation of $SU(3)_f$ symmetry. Another is that the 't Hooft-operator-induced spin-dependent forces have flavor ratios similar to the magnetic moment ratios (provided one ignores the difference between the onshell “constituent quark mass” and the determinantal masses m^* .) Therefore, one cannot trace their origin simply by the mass dependence.

Now let us define m^* in the Lagrangian coefficient, following [63], see also [64–66]. If there is a single instanton in the “empty” vacuum, as considered in the original 't Hooft paper, those are just quark masses m_q . The product of the quark masses is however also present in the instanton density (in this setting), and they all cancel out, leaving a finite Lagrangian even in the chiral limit $m_q \rightarrow 0$.

In an ensemble of instantons, the quark propagator in the QCD vacuum and restricted to the zero modes, is approximated by the form

$$S(x, y) = S_Z(x, y) + \sum_{I, J} \psi_{0I}^*(x) \left(\frac{1}{T} \right)_{I, J} \psi_{0J}(y) \quad (71)$$

where T_{IJ} denotes the so-called “instanton hopping” matrix, constructed out of the Dirac zero modes overlaps between neighboring instantons I, J . Note that it contributes as an *inverse* matrix, as propagators are inverse to Dirac operators. So, when one discusses a process in which both points x, y are inside the same instanton I^* , as per the definition of a hard block, we can restrict the sum to only the term with the zero mode of this very instanton. This leads to the following redefinition of the “determinantal mass”

$$\frac{1}{m_u} \equiv \left\langle \left(\frac{1}{T} \right)_{I^* I^*} \right\rangle. \quad (72)$$

Furthermore, in the diagrams containing *two* quark propagators of *different flavors* one has a different averaging

$$\frac{1}{m_{uudd}^2} \equiv \left\langle \left(\frac{1}{T} \right)_{I^* I^*}^2 \right\rangle. \quad (73)$$

These two quantities were evaluated in the random and interacting instanton liquid model, with

$$\frac{1}{m_u^2} \approx \frac{1}{(177 \text{ MeV})^2} \ll \frac{1}{m_{uudd}^2} \approx \frac{1}{(103 \text{ MeV})^2}. \quad (74)$$

The chief consequence of these substantial deviations from mean field can be captured by a “'t Hooft operator enhancement factor”

$$f_{\text{tHooft}} \equiv \left(\frac{m_u}{m_{uudd}} \right)^2 \approx 3. \quad (75)$$

This enhancement of a four-fermion operator relative to two-fermion squared has also been observed on the lattice in [27].

C. Spin and flavor-dependent interactions from zero modes

Since the 't Hooft induced interaction is nonlocal, there are additional contributions besides the local terms retained earlier. More specifically, for two flavors its generic form is

$$\begin{aligned} \mathcal{L} = & \kappa_2 A_{2N} \int \prod_{i=1}^4 \frac{d^4 k_i}{(2\pi)^4} \left(\frac{M(k_i)}{M(0)} \right)^{\frac{1}{2}} (2\pi)^4 \delta^4(k_1 + k_3 - k_2 - k_4) \\ & \times \frac{1}{2} e^{f_1 f_2} \epsilon^{g_1 g_2} (\bar{\psi}_{Rf_1}(k_1) \psi_{Lg_1}(k_2) \bar{\psi}_{Rf_2}(k_3) \psi_{Lg_2}(k_4) - 4B_{2N} \bar{\psi}_{Rf_1}(k_1) \sigma^a \psi_{Lg_1}(k_2) \bar{\psi}_{Rf_2}(k_3) \sigma^a \psi_{Lg_2}(k_4)) + (L \rightarrow R) \end{aligned} \quad (76)$$

with form factors, from a Fourier transform of the quark zero mode

$$\frac{M(k)}{M(0)} = \left(2z \left[I_0(z)K_1(z) - I_1(z)K_0(z) - \frac{1}{z}I_1(z)K_1(z) \right] \right)_{z=k\rho/2}^2. \quad (77)$$

We note that the antisymmetric operator for flavor exchange can be rewritten as

$$\epsilon^{f_1 f_2} \epsilon^{g_1 g_2} = \frac{1}{2} (\delta^{f_1 g_1} \delta^{f_2 g_2} - \tau^a{}_{f_1 g_1} \tau^a{}_{f_2 g_2}) \rightarrow \frac{1}{2} (1 - \tau_1 \cdot \tau_2) \quad (78)$$

so that (76) reads

$$\begin{aligned} \mathcal{L} = & \frac{1}{2} \kappa_2 A_{2N} \int \prod_{i=1}^4 \frac{d^4 k_i}{(2\pi)^4} \left(\frac{M(k_i)}{M(0)} \right)^{\frac{1}{2}} (2\pi)^4 \delta^4(k_1 + k_3 - k_2 - k_4) \\ & \times [(\bar{\psi}(k_1)\psi(k_2)\bar{\psi}(k_3)\psi(k_4) + \bar{\psi}(k_1)\gamma_5\psi(k_2)\bar{\psi}(k_3)\gamma_5\psi(k_4) \\ & - \bar{\psi}(k_1)\tau^a\psi(k_2)\bar{\psi}(k_3)\tau^a\psi(k_4) - \bar{\psi}(k_1)\tau^a\gamma_5\psi(k_2)\bar{\psi}(k_3)\tau^a\gamma_5\psi(k_4)) \\ & - 4B_{2N}(\bar{\psi}(k_1)\sigma^a\psi(k_2)\bar{\psi}(k_3)\sigma^a\psi(k_4) + \bar{\psi}(k_1)\sigma^a\gamma_5\psi(k_2)\bar{\psi}(k_3)\sigma^a\gamma_5\psi(k_4) \\ & - \bar{\psi}(k_1)\sigma^a\tau^b\psi(k_2)\bar{\psi}(k_3)\sigma^a\tau^b\psi(k_4) - \bar{\psi}(k_1)\sigma^a\tau^b\gamma_5\psi(k_2)\bar{\psi}(k_3)\sigma^a\tau^b\gamma_5\psi(k_4)]. \end{aligned} \quad (79)$$

Going ahead of ourselves, we note that in the sequel on the light-front Hamiltonian, we will use this operator with light-cone kinematics, *ultrarelativistic* on-shell spinor, in spin or chiral basis. In this paper, however, we are in the center-of-mass frame, in the nonrelativistic setting of a constituent quark model. Therefore, we perform the nonrelativistic reduction of (79) with on-mass-shell normalized Dirac spinors

$$U_s(p) = \begin{pmatrix} f(p)\chi_s \\ g(p)\sigma \cdot p\chi_s^C \end{pmatrix}, \quad V_s(p) = \begin{pmatrix} g(p)\sigma \cdot p\chi_s^C \\ f(p)\chi_s^C \end{pmatrix} \quad (80)$$

with standard normalization factors

$$f(p) = \left(\frac{E_p + m}{2E_p} \right)^{\frac{1}{2}} = (E_p + m)g(p) \quad (81)$$

and $E_p = (p^2 + m^2)^{\frac{1}{2}}$. For the reduction to central, spin-orbit, and spin-spin interactions, we set the kinematics in the center of mass defined in Fig. 14 with $k_1 = (E_{p+q}, \vec{p} + \vec{q})$, $k_2 = (E_p, \vec{p})$, $k_3 = (E_{p'-q}, \vec{p}' - \vec{q})$, $k_4 = (E_{p'}, \vec{p}')$, insert (80) into (79), and expand up to order p^2/m^2 . Recall that in a meson state $\vec{q}q$, the labels in Fig. 14 refer also to the flavor and spin $1, 2 \rightarrow U$ with mass m_Q for the quark, and $3, 4 \rightarrow V$ with mass $m_{\bar{Q}}$ for the antiquark. More specifically after setting $m = m_Q = m_{\bar{Q}}$, the order q^0/m^0 amounts to the two-body central and spin-spin operators

$$-\frac{1}{4} |\kappa_2| A_{2N} (1 - \tau_1 \cdot \tau_2) (1 - 16B_{2N} \vec{S}_1 \cdot \vec{S}_2) \quad (82)$$

in the U(1) or η' channel. For clarity, the form factor is temporarily set to 1 (zero size approximation). Taking into account the overall negative sign in κ_2 , and $16B_{2N} = 4/5$, and the values of $\vec{S}_1 \cdot \vec{S}_2 = -3/4$ for $S = 0$ states, one finds that the last bracket simplifies to $-8/5$ for the pseudoscalar (pion) channel. Note that (79) is only active in the $(\sigma, \pi, \sigma_5, \pi_5, \eta')$ channels. Equation (79) does not contribute to the vector channels.

The relativistic correction $\sim q^2/m^2$ amounts to the two-body operators (with again the form factor set to 1)

$$\begin{aligned} & -\frac{1}{4} |\kappa_2| A_{2N} (1 - \tau_1 \cdot \tau_2) \left(\frac{1}{4m^2} \right) (-L_S - 4S_T \\ & + 4B_{2N} (3L_S + 4S_T + 8q^2 S_1 \cdot S_2)) \end{aligned} \quad (83)$$

with spin-orbit and tensor operators

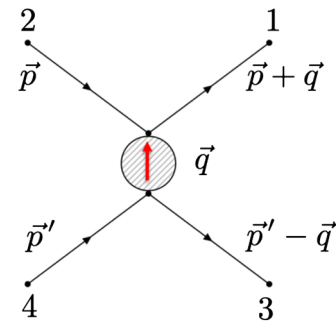


FIG. 14. Kinematics in the center-of-mass frame of the two-flavor instanton induced interaction with in-out on-shell Dirac fermions.

$$L_S = (S_1 + S_2) \cdot (iq \times (p - p')),$$

$$S_T = S_1 \cdot qS_2 \cdot q, \quad S_{12} = 3(S_1 \hat{q})(S_2 \hat{q}) - (S_1 S_2), \quad (84)$$

with L_S symmetrized using $\vec{p} + \vec{p}' = 0$. The translation $iq \rightarrow \nabla$ to configuration space will be understood.

D. Zero-mode-induced potential for pions

In Sec. IV A we have already studied the pion case, and defined the value of the 't Hooft effective coupling (63) needed to put the pion at the empirical mass. The first question we now discuss is whether the ILM (component of the instanton ensemble) can provide a coupling of this magnitude. The answer to this question is affirmative.

The “determinantal masses” induced by the quark condensates are given by the following expressions for light and strange quarks:

$$m_q^* = \frac{2\pi^2 \rho^2}{3} |\langle \bar{q}q \rangle|, \quad m_s^* = \frac{2\pi^2 \rho^2}{3} |\langle \bar{s}s \rangle| + m_s. \quad (85)$$

Using them, for a fixed instanton radius $\rho = 0.33 \text{ fm} \approx 1.4 \text{ GeV}^{-1}$, we get the following value of the coupling of $\bar{u}d\bar{u}$ 't Hooft vertex:

$$G_{ud} = A_{2N} \frac{3n}{8} \frac{(4\pi^2)^3 \rho^9}{(m_q^*)^2 (m_s^*)} |\langle \bar{s}s \rangle| \approx 27 \text{ GeV}^{-2}. \quad (86)$$

It is larger than the value of 17 GeV^{-2} we fitted from the pion mass using the Schrödinger equation above, by about 50%. However, note that it contains a large (sixth) power of the instanton size, which is not yet defined with sufficiently high precision. The numbers would match if one reduced it from $1/3$ to 0.29 fm .

Now, assuming that the 't Hooft-induced potential puts the pion at the right mass, we now turn our attention to the ρ meson. In the previous section we have found that there is an attractive 't Hooft-induced potential which, at the leading nonrelativistic order (82), is just *half* of that for the pion. Naively, one might think that this potential will pull the mass of the ρ to *half* of what it does to the pion, putting it right at the experimentally observed value. Unfortunately, that is not the case. The effects of the 't Hooft operator are too large to be treated as small perturbations. A factor of 2 difference in a potential does not imply a factor of 2 in the energy, because the wave function itself depends strongly on it. What we found is that, due to the 't Hooft-induced potential, the pion's size gets reduced, making it comparable to the instanton potential range $\sim \rho$. Half of it, acting against the repulsive $V_{SS(r)}$ from the earlier contributions, fails to shrink the ρ size, which remains roughly twice the size of π . This reduces the wave function at small distances roughly by a factor of 2^3 , and effectively reduces the matrix element of

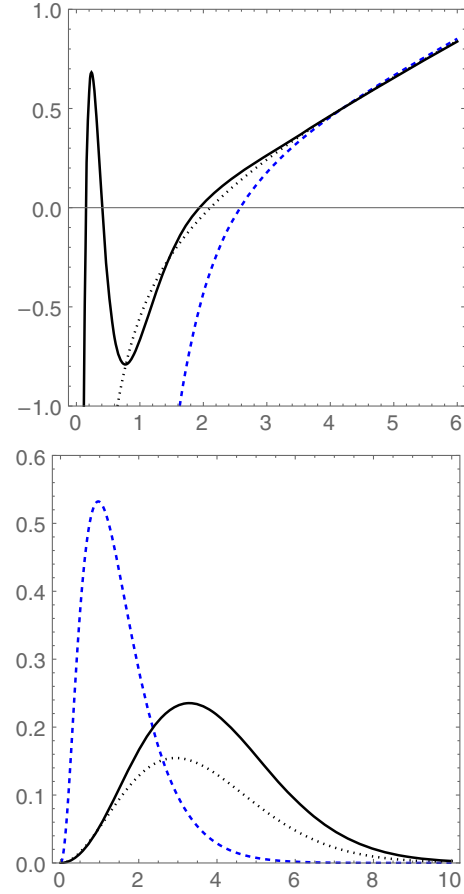


FIG. 15. The total potentials including the 't Hooft ones (top) and wave functions as $r^2\psi(r)^2$ (bottom) for the ρ channel (solid curves), the π channel (blue dashed curves), and the generic Cornell potential (black dots). All potentials are shown versus the distance r in GeV^{-1} .

the $V^{\text{Hooft}}(r)$ in the ρ case by a comparable factor. The corresponding potentials and wave functions are shown in Fig. 15.

E. The ρ meson and the “molecule-induced” potential

This leaves us with the model prediction for the ρ meson mass m_ρ in the vicinity of the mass following from a “generic Cornell meson,” with $m \approx 1.4 \text{ GeV}$, far from its experimental mass. The theory part is missing something very important for the vector light quark channel.

Fortunately, there is still one more effect, already discussed in the literature, the second-order 't Hooft effective forces due to “molecular” configurations; see the lower plot in the Introduction, Fig. 1. In particular, the effective Lagrangian induced by these molecules was used in the theory of color superconductivity at high density [67], from which we borrow its analytic form

$$\begin{aligned}
 L_{\text{mol}}/G_{\text{mol}} &= \frac{1}{N_c^2} [(\bar{\psi}\gamma_\mu\psi)^2 + (\bar{\psi}\gamma_\mu\gamma_5\psi)^2] - \frac{1}{2N_c(N_c-1)} [(\bar{\psi}\gamma_\mu\lambda^a\psi)^2 + (\bar{\psi}\gamma_\mu\gamma_5\lambda^a\psi)^2] \\
 &\quad - \frac{1}{N_c^2} [(\bar{\psi}\gamma_\mu\psi)^2 - (\bar{\psi}\gamma_\mu\gamma_5\psi)^2] - \frac{2N_c-1}{2N_c(N_c^2-1)} [(\bar{\psi}\gamma_\mu\lambda^a\psi)^2 - (\bar{\psi}\gamma_\mu\gamma_5\lambda^a\psi)^2]. \quad (87)
 \end{aligned}$$

It follows by using the same color orientation for the instanton and anti-instanton, which locks them to their most attractive channel. The quark fields come from zero modes of I and \bar{I} , so there is no Pauli principle and the flavors can be both the same or different. Note that in this case the chiralities of the quarks and antiquarks are the same in each term, which is suitable for the ρ meson channel. Choosing the vector $\gamma_\mu\lambda^a$ terms and reducing the color matrices for the meson case, we can reduce it to

$$L_{\text{mol}} = G_{\text{mol}}(\bar{u}\gamma_\mu u)_x(\bar{d}\gamma_\mu d)_y F_{\text{mol}}(x-y) \quad (88)$$

where we introduced another form factor to account for the nonlocality of the instanton–anti-instanton molecule. In principle, one can evaluate (88) in a way that is analogous to our treatment of the 't Hooft Lagrangian. However, it would now include *two* four-dimensional integrations over positions of both centers, plus the relatively complicated $\bar{I}\bar{I}$ interaction depending on the relative color orientations. Qualitatively, one expects its nonlocality size to approximately double, so we may just substitute the instanton size $\rho \rightarrow 2\rho$ in the instanton form factor as an estimate. As a result, its coefficient is reduced by $1/2^3$ in the form factor (C1). Such a size reduction of the potential range is precisely what is needed to obtain the correct ρ meson mass.

More specifically, setting the corresponding potential into the Schrödinger equation, along with the Cornell and

spin-spin terms, we find that the correct ρ mass is indeed obtained for

$$\frac{G_{\text{mol}}}{G_{\text{Hooft}}} = \frac{120 \text{ GeV}^2}{17 \text{ GeV}^2} \sim \frac{n_{\text{mol}} + n_{\text{ILM}}}{n_{\text{ILM}}} \approx 7. \quad (89)$$

Note that this ratio of couplings (or densities) agrees well with what was deduced from the central potential fitting the linear potential discussed above.

(As a parting comment, we remind the reader that the NJL model—the pioneering effort to describe chiral symmetry breaking and nonperturbative interactions in hadrons—involves flavor-diagonal terms like the one we used here. In later papers based on the NJL model, those contributions were attributed to the “strong coupling part” of one gluon exchange.)

F. Zero mode effects in heavy-light systems

The spin interactions for heavy-light quarks split into the contributions solely from the nonzero modes which give rise to the same general spin-dependent interactions as in (40).

For simplicity, we start with the heavy-light mesons, with a single light quark. The contributions to the quark propagators come from the zero mode for the light quark, and the nonzero modes for the heavy quark. The resulting spin-independent interaction was derived in [61]

$$\mathcal{L}_{qQ} = -\left(\frac{\Delta m_Q \Delta m_q}{2nN_c}\right) \left(\bar{Q} \frac{1+\gamma^0}{2} \mathbf{Q} \bar{q} \mathbf{q} + \frac{1}{4} \bar{Q} \frac{1+\gamma^0}{2} \lambda^a \mathbf{Q} \bar{q} \lambda^a \mathbf{q}\right) \quad (90)$$

while the spin-dependent interaction is more suppressed,

$$\mathcal{L}_{qQ}^{\text{spin}} = -\left(\frac{\Delta m_Q^{\text{spin}} \Delta m_q}{2nN_c}\right) \times \frac{1}{4} \left(\bar{Q} \frac{1+\gamma^0}{2} \lambda^a \sigma^{\mu\nu} \mathbf{Q} \bar{q} \lambda^a \sigma^{\mu\nu} \mathbf{q}\right) \quad (91)$$

with $\Delta m_Q^{\text{spin}}/\Delta m_q \sim 1/100$ (charm). The local potential stemming from (90) and (91) is

$$V_{qQ}(r) = \left(\frac{\Delta m_Q \Delta m_q}{2nN_c}\right) \left(1 + \frac{1}{4} \lambda_q^a \lambda_Q^a\right) \delta^3(r). \quad (92)$$

In the mesons, the colors on the two lines are opposite and the second term dominates the first, so this local potential is negative. For the D meson it amounts to $\langle V_{qQ} \rangle \approx -180 \text{ MeV}$ [61], to be compared with the nonrelativistic

energy due to the standard Hamiltonian, kinetic plus central potential average

$$\langle P^2/2m_q + V_c(r) \rangle \approx +250 \text{ MeV}.$$

The spin-spin potential is

$$V_{qQ}^{\text{spin}}(r) = -\left(\frac{\Delta m_Q^{\text{spin}} \Delta m_q}{2nN_c}\right) S_q \cdot S_Q \lambda_q^a \lambda_Q^a \delta^3(r). \quad (93)$$

For the D meson both the relative spin and color are negative, so the contribution of this term is negative as well, giving $\langle V_{qQ}^{\text{spin}} \rangle \approx -42$ MeV [61]. The contribution of this term to the spin splitting is then

$$M(D^*) - M(D) = (4/3)42 \text{ MeV} = 56 \text{ MeV}$$

to be compared with our calculations above giving together $\langle V_{SS}^{\text{pert}} + V_{SS}^{\text{inst}} \rangle \approx 96$ MeV. We thus conclude that all three contributions together—the perturbative one and the two instanton-induced ones—do finally reproduce this mass difference, close to the experimental value $M(D^*) - M(D) = 137$ MeV.

V. SUMMARY AND DISCUSSION

The purpose of this work, the first in a series, is to relate the current views on the QCD vacuum with the quark-antiquark forces (both central and spin-dependent ones), known to us via spectroscopy of nonrelativistic quarkonia and other mesons.

While most of our efforts in the series will focus on the light-front formulation, in this paper we addressed the mesonic spectroscopy in its center-of-mass frame. Its main theory content is the reformulation of the 40-year-old “dilute instanton liquid model,” parametrized in (6). Unlike previous studies [which mostly focused on the spontaneous breaking of $SU(N_f)_a$ chiral symmetry and explicit breaking of $U(1)_a$, pions and η' and instanton fermionic zero modes] we now focus on the vacuum average of Wilson lines, without and with additional field strength insertions. The novel element is the inclusion of “incomplete tunneling events,” or $\bar{I}\bar{I}$ “molecules.” Including those, one finds that the instanton-induced contribution to the static central potential is nearly linear, and can reproduce the magnitude of the phenomenological potential up to distances $r < 0.8$ fm. This normalization of the “molecule density” crudely corresponds to the lowest lattice extrapolations of Fig. 2(b) of Ref. [42] to zero cooling time (that is, to the physical vacuum). We have referred to this model as the *dense instanton liquid* with a diluteness parameter $\kappa \sim 1$. The density of molecules is $n_{\text{mol}} = 6 \text{ fm}^{-4}$.

This novel model has nontrivial predictive power: unlike the electric flux tube model, instantons are self-dual and include magnetic field strength as large as the electric ones. One therefore can calculate the instanton-induced spin-dependent forces. The setting is explained in Fig. 10. Using uncorrelated instantons, we found the spin-spin, spin-orbit, and tensor forces shown in the lower part of Fig. 9. In particular the spin-spin potential V_{SS} in Fig. 12 shows that the instanton-induced potential (blue dashed line) is comparable to the perturbative potential (black dash-dotted line). Their combined area agrees with the lattice result (black solid line). The matrix elements of V_{SS} are compared with the experimental splittings of the $1S$ mesons (e.g.

$J/\psi - \eta_c$) in Table II, with good agreement. We emphasize that there are no free parameters in this calculation.

Another observation from Fig. 12, shows that instantons of “standard” size $\rho = 1/3$ fm produce a V_{SS} potential of a correct area but larger range, in comparison to lattice results. We have shown that incorporating the structure of the magnetic fields stemming from the instanton-anti-instanton molecules (see Fig. 13 and related discussion) cures this problem.

Moving from the $1S$ shell (with two states $J = 0, 1$) to the $1P$ shell (with four states), we carried similar comparison using the matrix elements of all three spin-dependent potentials. We have evaluated the matrix elements of all three potentials, both perturbative and instanton induced. As shown in Table III, here the situation is much more complex, and a good agreement between theory and the empirical values is not achieved. In particular, a large empirical value of the spin-orbit force is an order of magnitude above both the perturbative and instanton-induced matrix elements. The reasons why the $1P$ shell splitting is not reproduced remains unclear, although we suspect that it may be related to the negative spin-orbit contribution from the string, to be discussed in paper II [1] later in this series. Clearly more work is required, especially on the lattice side.

Although our straightforward evaluation of the perturbative and instanton-induced potentials have not reproduced the apparently negative tensor force for light quarks, the negative *sign* of the instanton-induced term indicates that, with some play of parameters, it may be done.

Let us also mention that we will return to the spin-dependent forces *on the light front* in paper III [2], discussing in detail the quadrupole moment of the vector mesons. The issue of the instanton-induced interquark forces will be studied for the three quark case (baryons) in paper IV [3].

While for heavy quarks the spin forces as given by Wilson lines are sufficient, for light quarks there exists extra “anomalous” processes, in which quarks do not travel continuously in time, but are instead dumped into the Dirac sea and substituted by another quark, with *opposite chirality*. The nonrelativistic reduction of a six-quark 't Hooft operator has produced novel spin-dependent forces. Their application to the pion case is successful, as well as to the heavy-light systems. The effects related to the zero modes and the 't Hooft effective interactions can still be put in the form of quasilocal flavor-nondiagonal potentials, i.e. central and spin dependent. The phenomenological implications of this is a reminder of the *two-component* instanton model discussed here, meaning that for the 't Hooft potential the instanton density is the smaller one, taken from the original ILM. The magnitude of such 't Hooft potential is found of the size needed to put the pion mass at its small physical value. It is in agreement with the long-known view of the pion as depicted in the top panel of Fig. 1.

A significant part of this work is devoted to two alternative description of instanton–anti-instanton configurations, or “molecules” for short. As we show in Fig. 13 and the text around it, using their fields in Wilson lines does modify the shape of spin-dependent forces, making them shorter range. Yet this part is open ended in the sense that it is intended for future quantitative calculations of the potentials.

As a parting comment, novel interpretations of inter-quark potentials we propose in this paper need and should be tested. One way to do this is to calculate corresponding potentials on the lattice and compare the results from a full vacuum field ensemble to those *during* a gradient flow cooling process, eventually with only an instanton remaining. This will allow one to single out molecular and single instanton-induced contributions.

ACKNOWLEDGMENTS

This work was supported by the U.S. Department of Energy Office of Science under Contract No. DE-FG-88ER40388.

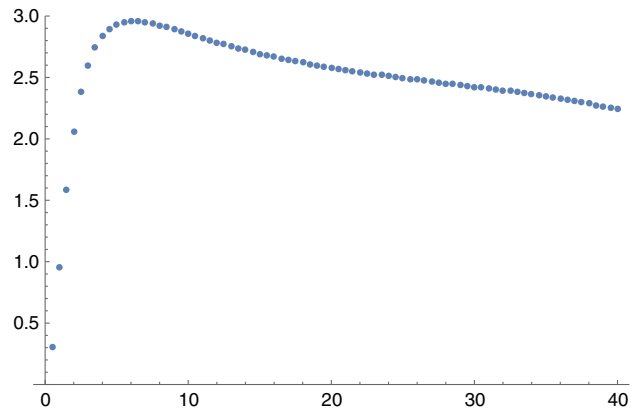


FIG. 16. $I(x)$ versus x as given in (4).

APPENDIX A: ASYMPTOTICS OF $V_C(r)$

The instanton-induced central potential $V_C(r)$ in Fig. 4 asymptotes twice the self-energy $2\Delta m_Q$. This asymptotics is reached from *above* in singular gauge contrary to expectations. The simplest way to see this, is to note that

$$2\Delta M_{Q\rho} = \frac{8\pi n\rho^4}{N_c} \int_0^\infty dy y^2 \left(1 + \cos\left(\frac{\pi y}{\rho^2 + y^2}\right) \right) \approx \frac{8\pi n\rho^4}{N_c} 2.2 \quad (\text{A1})$$

is substantially smaller than the potential in Fig. 4. A numerical evaluation of $I(x)$ as in (18) at large x , is shown in Fig. 16. It confirms that the asymptotics is slowly reached from above.

We note that a Taylor expansion of the integrand in $I(x)$ suggests $1/r^3$ as the leading contribution, but the remaining integration is divergent, thereby invalidating the expansion. In [68] it was suggested that the asymptotics is reached from below through $-\pi^2/2r$. This result is correct in a perturbative regular gauge with no additional color rotations, but not in a nonperturbative singular gauge with additional color rotations. Also, the $1/r$ central potential yields a spin-spin potential $V_{SS}(r)$ as a delta function which is also not compatible with the $1/r^2$ behavior noted above. Figure 16 can be fitted numerically by $2\Delta M_Q + C/r^p$ with

$p \ll 1$ and $C > 0$. Its ensuing Laplacian then gives $p(1-p)/r^{2+p}$, which is consistent with $V_{SS}(r)$ at large r .

APPENDIX B: DEFINITIONS OF THE SPIN-DEPENDENT POTENTIALS

Following Ref. [11], we give for completeness the correlation functions generating the five spin-dependent potentials. The integrals over points z, z' are taken along two Wilson lines located at \vec{x}_1, \vec{x}_2 and running in the Euclidean time direction, from $-T/2$ to $T/2$. The limit of large $T \rightarrow \infty$ is not written explicitly but assumed. The normalization to $\langle 1 \rangle$ means subtraction of the central potential coming from the correlator of Wilson lines without the extra field strengths

$$\begin{aligned} \frac{r^k}{r} \frac{dV_1(r)}{dr} &= \epsilon_{ijk} \int dz dz' \left(\frac{z-z'}{T} \right) \frac{g^2}{2} \langle B^i(\vec{x}_1, z) E^j(\vec{x}_1, z') \rangle / \langle 1 \rangle, \\ \frac{r^k}{r} \frac{dV_2(r)}{dr} &= \epsilon_{ijk} \int dz dz' \left(\frac{z-z'}{T} \right) \frac{g^2}{2} \langle B^i(\vec{x}_2, z) E^j(\vec{x}_1, z') \rangle / \langle 1 \rangle \\ &\times [(\hat{r}^i \hat{r}^j - \delta_{ij}/3) V_3(r) + \delta_{ij}/3] V_4(r) = \int dz dz' \frac{g^2}{T} \langle B^i(\vec{x}_2, z) E^j(\vec{x}_1, z') \rangle / \langle 1 \rangle. \end{aligned} \quad (\text{B1})$$

Although it involves only the vector product of electric and magnetic fields, using the Bianchi identity one can express it via a correlator of two B fields, as expected for nonrelativistic spin interactions. It is however of little importance for instantons, which are (anti-)self-dual $\vec{E} = \pm\vec{B}$.

Note that the reduction of the dressed Wilson line “WEW” line with an electric field insertion can be made into a derivative of the Wilson line over its location, via the following steps:

$$\begin{aligned}
& D_m(y)\mathbf{W}(x_0, y_0) - \mathbf{W}(x_0, y_0)D_m(y) \\
&= \langle x_0 | D_0 \frac{1}{iD_0} - \frac{1}{iD_0} D_m | y_0 \rangle \\
&= \langle x_0 | \frac{1}{iD_0} [iD_0, D_m] \frac{1}{iD_0} | y_0 \rangle \\
&= \langle x_0 | \frac{1}{iD_0} (-F_{0m}) \frac{1}{iD_0} | y_0 \rangle \\
&= \int_{-\frac{1}{2}T}^{+\frac{1}{2}T} dz_0 \mathbf{W}(-T, z_0) (-F_{0m})(z_0) \mathbf{W}(z_0, T) \quad (\text{B2})
\end{aligned}$$

and in the large $|T| \rightarrow \infty$ asymptotic the field is assumed to vanish, so the covariant derivative can be changed to an ordinary one.

Subsequent discussions of the $\mathcal{O}(1/m^2)$ of the potentials have been made, starting from complete effective actions of NRQCD and pNRQCD to this order, and some modifications of the expressions in [11] were found (see Eqs. (49)–(51) in [5]). Modulo matching, the only difference was noted in the spin-orbit coefficient with no $\frac{1}{2}$ in (B1). However, for the purposes of our work, it is enough to note that the spin-spin and spin-orbit potentials are related to the correlators of two magnetic fields, and the spin orbit to the correlator of electric and magnetic fields. (Of course,

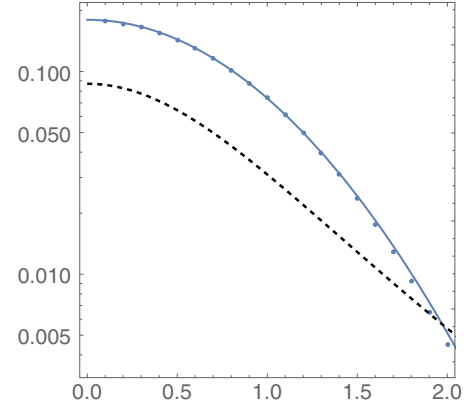


FIG. 17. Numerically integrated and normalized integral (C1) (points), compared to a fit (solid line). Also for comparison we show (dashed line) the normalized “smoothed delta function” as used in (49) for $\delta = \rho$. It was our initial choice, but as shown here, it does not provide an accurate description of the form factor and therefore is not used.

the correlators include the appropriate Wilson lines, and are integrated over the time difference between the field strengths.)

APPENDIX C: FORM FACTOR IN THE ‘T HOOFT LAGRANGIAN

In many applications, the instanton induced form factor on the tunneling quarks is used in the momentum representation, more specifically, as the Fourier transform of the zero modes in (77). However, in the effective potential we use, there are four zero modes, thus the fourth power of $M(k)$. Its inverse Fourier transform to coordinate space is complicated. We use instead directly the coordinate expression, with two *densities* of zero modes separated by a distance r , with the explicit integration over the location of the instanton center z_μ

$$\begin{aligned}
F(r) &\sim \int d^4z |\psi_0(z^\mu - r^\mu/2)|^2 |\psi_0(z^\mu + r^\mu/2)|^2 \\
&\sim \int \frac{z^3 dz \sin^2(\theta) d\theta}{(z^2 + r^2/4 + zr \cos(\theta) + \rho^2)^3 (z^2 + r^2/4 - zr \cos(\theta) + \rho^2)^3} \approx 0.18 \exp(-0.89r^2). \quad (\text{C1})
\end{aligned}$$

The last expression is a fit, normalized by $\int d^3F(r) = 1$, with our standard size $\rho = 1.4 \text{ GeV}^{-1}$. The comparison between the numerical integral and the fit is shown in Fig. 17.

APPENDIX D: FIELD STRENGTHS THROUGH CONFORMAL MAPPING

The field strength F_{MN} and its dual $\star F_{MN}$ for the tunneling at fixed energy in $O(4)$ symmetric form (Step 1) are given by

$$\begin{aligned}
y^2 \vec{E} &= \vec{\sigma} \left(f' - \frac{(\vec{y})^2}{y^2} (f' - 2f\bar{f}) \right) \\
&\quad + \frac{(\vec{y} \cdot \vec{\sigma} \vec{y} - y_4 \vec{\sigma} \times \vec{y})}{y^2} (f' - 2f\bar{f}), \\
y^2 \vec{B} &= \vec{\sigma} \left(2f\bar{f} + \frac{(\vec{y})^2}{y^2} (f' - 2f\bar{f}) \right) \\
&\quad - \frac{(\vec{y} \cdot \vec{\sigma} \vec{y} - y_4 \vec{\sigma} \times \vec{y})}{y^2} (f' - 2f\bar{f}), \quad (\text{D1})
\end{aligned}$$

with $E^i = F^{i4}$ and $B^i = \frac{1}{2} \epsilon^{ijk} F^{jk}$. For self-dual fields $f' = 2f\vec{f}$ and $\vec{E} = \vec{B}$ are hedgehogs in color spin as expected for the instanton path. For the sphaleron path, we have $f = \frac{1}{2}$ and

$(\vec{E} + \vec{B}) = \vec{\sigma}/2y^2$, as only the electric plus magnetic field sum is hedgehog in color spin. We then use the conformal (stereographic) map (Step 2), as explained in the text.

-
- [1] E. Shuryak and I. Zahed, following paper, *Phys. Rev. D* **107**, 034024 (2023).
- [2] E. Shuryak and I. Zahed, this issue, *Phys. Rev. D* **107**, 034025 (2023).
- [3] E. Shuryak and I. Zahed, this issue, *Phys. Rev. D* **107**, 034026 (2023).
- [4] E. Shuryak and I. Zahed, this issue, *Phys. Rev. D* **107**, 034027 (2023).
- [5] A. Pineda and A. Vairo, *Phys. Rev. D* **63**, 054007 (2001); **64**, 039902(E) (2001).
- [6] N. Brambilla, G. A. Krein, J. Tarrús Castellà, and A. Vairo, *Phys. Rev. D* **97**, 016016 (2018).
- [7] J. F. Arvis, *Phys. Lett.* **127B**, 106 (1983).
- [8] O. Aharony and N. Klinghoffer, *J. High Energy Phys.* **12** (2010) 058.
- [9] A. Athenodorou and M. Teper, *J. High Energy Phys.* **12** (2021) 082.
- [10] C. G. Callan, Jr., R. F. Dashen, D. J. Gross, F. Wilczek, and A. Zee, *Phys. Rev. D* **18**, 4684 (1978).
- [11] E. Eichten and F. Feinberg, *Phys. Rev. D* **23**, 2724 (1981).
- [12] T. Schäfer and E. V. Shuryak, *Rev. Mod. Phys.* **70**, 323 (1998).
- [13] Y. Nambu and G. Jona-Lasinio, *Phys. Rev.* **122**, 345 (1961).
- [14] M. A. Shifman, A. I. Vainshtein, and V. I. Zakharov, *Nucl. Phys.* **B147**, 385 (1979).
- [15] V. A. Novikov, M. A. Shifman, A. I. Vainshtein, and V. I. Zakharov, *Nucl. Phys.* **B191**, 301 (1981).
- [16] E. V. Shuryak, *Rev. Mod. Phys.* **65**, 1 (1993).
- [17] A. A. Belavin, A. M. Polyakov, A. S. Schwartz, and Y. S. Tyupkin, *Phys. Lett.* **59B**, 85 (1975).
- [18] E. V. Shuryak, *Nucl. Phys.* **B198**, 83 (1982).
- [19] D. B. Leinweber, [arXiv:hep-lat/0004025](https://arxiv.org/abs/hep-lat/0004025).
- [20] J. C. Biddle, W. Kamleh, and D. B. Leinweber, *Phys. Rev. D* **102**, 034504 (2020).
- [21] J. C. Biddle, W. Kamleh, and D. B. Leinweber, *EPJ Web Conf.* **245**, 06010 (2020).
- [22] I. Zahed, *Phys. Rev. D* **104**, 054031 (2021).
- [23] G. 't Hooft, *Phys. Rev. D* **14**, 3432 (1976); **18**, 2199(E) (1978).
- [24] E. V. Shuryak, *Nucl. Phys.* **B203**, 140 (1982).
- [25] L. Y. Glozman, C. B. Lang, and M. Schrock, *Phys. Rev. D* **86**, 014507 (2012).
- [26] M. C. Chu, J. M. Grandy, S. Huang, and J. W. Negele, *Phys. Rev. D* **49**, 6039 (1994).
- [27] P. Faccioli and T. A. DeGrand, *Phys. Rev. Lett.* **91**, 182001 (2003).
- [28] D. M. Ostrovsky, G. W. Carter, and E. V. Shuryak, *Phys. Rev. D* **66**, 036004 (2002).
- [29] F. R. Klinkhamer and N. S. Manton, *Phys. Rev. D* **30**, 2212 (1984).
- [30] E.-M. Ilgenfritz and E. V. Shuryak, *Nucl. Phys.* **B319**, 511 (1989).
- [31] R. Rapp, T. Schäfer, E. V. Shuryak, and M. Velkovsky, *Phys. Rev. Lett.* **81**, 53 (1998).
- [32] E. Shuryak and I. Zahed, *Phys. Rev. D* **103**, 054028 (2021).
- [33] Y. Liu and I. Zahed, [arXiv:2102.07248](https://arxiv.org/abs/2102.07248).
- [34] E. V. Shuryak, *Nucl. Phys.* **B302**, 621 (1988).
- [35] I. I. Balitsky and A. V. Yung, *Phys. Lett.* **168B**, 113 (1986).
- [36] A. V. Yung, *Nucl. Phys.* **B297**, 47 (1988).
- [37] J. J. M. Verbaarschot, *Nucl. Phys.* **B362**, 33 (1991); **B386**, 236(E) (1992).
- [38] V. V. Khoze and A. Ringwald, preprint CERN-TH-6082-91 (1991).
- [39] E. V. Shuryak and J. J. M. Verbaarschot, *Phys. Rev. Lett.* **68**, 2576 (1992).
- [40] E. Shuryak and I. Zahed, [arXiv:2102.00256](https://arxiv.org/abs/2102.00256).
- [41] M. Luscher and P. Weisz, *J. High Energy Phys.* **02** (2011) 051.
- [42] A. Athenodorou, P. Boucaud, F. De Soto, J. Rodríguez-Quintero, and S. Zafeiropoulos, *J. High Energy Phys.* **02** (2018) 140.
- [43] P. Boucaud, F. De Soto, A. Le Yaouanc, J. P. Leroy, J. Micheli, H. Moutarde, O. Pene, and J. Rodríguez-Quintero, *J. High Energy Phys.* **04** (2003) 005.
- [44] E. V. Shuryak and I. Zahed, *Phys. Rev. D* **62**, 085014 (2000).
- [45] M. Giordano and E. Meggiolaro, *Phys. Rev. D* **78**, 074510 (2008).
- [46] M. Giordano and E. Meggiolaro, *Phys. Rev. D* **81**, 074022 (2010).
- [47] U. T. Yakhshiev, H.-C. Kim, M. M. Musakhanov, E. Hiyama, and B. Turimov, *Chin. Phys. C* **41**, 083102 (2017).
- [48] E. V. Shuryak, *Nucl. Phys.* **B203**, 93 (1982).
- [49] Y. Liu, M. A. Nowak, and I. Zahed, *Phys. Rev. D* **100**, 126023 (2019).
- [50] Y. Liu, M. A. Nowak, and I. Zahed, *Phys. Rev. D* **105**, 054021 (2022).
- [51] M. Luscher, *Phys. Lett.* **70B**, 321 (1977).
- [52] B. M. Schechter, *Phys. Rev. D* **16**, 3015 (1977).
- [53] V. A. Rubakov, D. T. Son, and P. G. Tinyakov, *Phys. Lett. B* **287**, 342 (1992).
- [54] D. Gromes, *Z. Phys. C* **26**, 401 (1984).
- [55] W. Buchmüller, *Phys. Lett.* **112B**, 479 (1982).
- [56] R. D. Pisarski and J. D. Stack, *Nucl. Phys.* **B286**, 657 (1987).
- [57] Y. Koma and M. Koma, *Nucl. Phys.* **B769**, 79 (2007).
- [58] T. Kawanai and S. Sasaki, *Phys. Rev. D* **92**, 094503 (2015).
- [59] T. Barnes, S. Godfrey, and E. S. Swanson, *Phys. Rev. D* **72**, 054026 (2005).

- [60] J. Koponen, A. C. Zimmermann-Santos, C. T. H. Davies, G. P. Lepage, and A. T. Lytle, *Phys. Rev. D* **96**, 054501 (2017).
- [61] S. Chernyshev, M. A. Nowak, and I. Zahed, *Phys. Rev. D* **53**, 5176 (1996).
- [62] E. V. Shuryak and J. L. Rosner, *Phys. Lett. B* **218**, 72 (1989).
- [63] P. Faccioli and E. V. Shuryak, *Phys. Rev. D* **64**, 114020 (2001).
- [64] H. Forkel and M. Nielsen, *Phys. Lett. B* **345**, 55 (1995).
- [65] A. Blotz and E. V. Shuryak, *Phys. Rev. D* **55**, 4055 (1997).
- [66] V. V. Braguta and A. I. Onishchenko, *Phys. Lett. B* **591**, 255 (2004).
- [67] R. Rapp, T. Schäfer, E. V. Shuryak, and M. Velkovsky, *Ann. Phys. (N.Y.)* **280**, 35 (2000).
- [68] U. T. Yakhshiev, H.-C. Kim, M. M. Musakhanov, E. Hiyama, and B. Turimov, *Chin. Phys. C* **41**, 083102 (2017).